Catalysis Letters (2025) 155:378
https://doi.org/10.1007/s10562-025-05207-1

Catalytic Application of a Zwitterionic Polymeric Network for Hydrogen Generation via Sodium Borohydride Methanolysis

Kutalmis Gokkus[1] · Sefika Kaya[2] · Mahmut Gür[3] · Derya Yildiz[2] · Erol Yıldırım[4] · Hilal Kivrak[2] et al. ***[full author details at the end of the article]***

Received: 12 July 2025 / Accepted: 29 September 2025 / Published online: 30 October 2025

Abstract

Hydrogen energy is widely regarded as one of the most promising alternatives to fossil fuels. This study focuses on the synthesis of an environmentally friendly zwitterionic polymer catalyst, Poly(Quaternized-2-diethylaminoethyl methacrylate) (P(Q-DMA)), was synthesized and evaluated for the first time as a metal-free catalyst in $NaBH_4$ methanolysis for hydrogen production. Owing to its zwitterionic nature, P(Q-DMA) was designed to interact synergistically with methanol and sodium borohydride through multiple mechanisms, including ion–dipole, ion–ion, and hydrogen-bonding interactions. The structure–function relationship was investigated using surface analysis (BET, SEM and Zeta), chemical characterization (FTIR, TGA), and kinetic modeling. Systematic optimization revealed high catalytic efficiency, achieving a hydrogen generation rate (HGR) of 443.4 mL H_2 min^{-1} $gcat^{-1}$ and a mass-specific HGR of 8868.4 mL H_2 min^{-1} $gcat^{-1}$, with a low activation energy (Ea) of 19.91 kJ mol^{-1}. The polymer also exhibited good electrocatalytic activity (0.72 mA cm^{-2} at 0.8 V in 1 M NaOH + 0.1 M $NaBH_4$) and stable performance during $NaBH_4$ electrooxidation. Importantly, zeta potential values shifted from + 13.1 mV before reaction to − 12.2 mV (unwashed) and − 8.43 mV (washed) after reaction, indicating surface modification by adsorbed borate species. These results highlight P(Q-DMA) as a promising biocompatible, metal-free catalyst for scalable hydrogen production and electrochemical applications, aligning with sustainable and clean energy goals.

Graphical Abstract

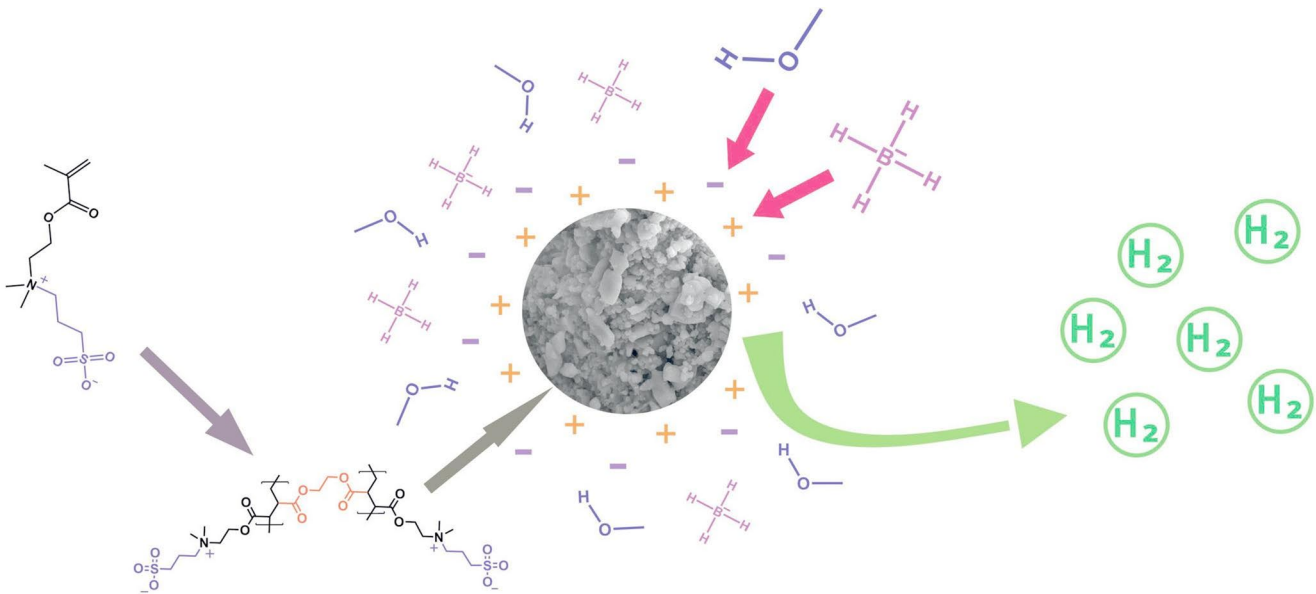

Keywords Low activation energy · $NaBH_4$ methanolysis · Zwitterionic polymer catalyst · Renewable energy · Sustainable catalysis · Hydrogen generation

✉

1 Introduction

Hydrogen production has become a cornerstone of the global transition to sustainable energy systems. Among the available methods, the methanolysis of $NaBH_4$ has attracted significant attention because of its high hydrogen yield under relatively mild reaction conditions. $NaBH_4$, a white crystalline solid with high hydrogen content and remarkable stability, is considered a leading candidate for efficient hydrogen storage and release [1]. In reaction with methanol (MeOH), $NaBH_4$ undergoes methanolysis, producing hydrogen gas according to the following equation [2]:

$$NaBH_4 + 4CH_3OH \rightarrow NaB(OCH_3)_4 + 4H_{2(g)}$$

Despite its potential, this reaction is inherently slow, necessitating the use of catalysts to accelerate the process by facilitating interactions among $NaBH_4$ and MeOH while reducing the activation energy Effective catalysts enhance the physical and chemical interactions in the reaction medium, enabling rapid hydrogen production.

The methanolysis reaction involves three critical components: the catalyst, MeOH, and $NaBH_4$. The interaction among these components governs the reaction rate. For example, BH_4^- is an anion and forms strong ion–ion interactions and hydrogen bonds with cations and heteroatoms, respectively, in the reaction medium. MeOH contains a highly electronegative oxygen atom and therefore exhibits strong ion–dipole interactions with other molecules. It is also well known that -OH groups can form strong hydrogen bonds. Therefore, a catalyst capable of simultaneously exhibiting ion–dipole, ion–ion, and hydrogen-bonding interactions with $NaBH_4$ and MeOH would theoretically be highly effective. Consequently, many studies have been conducted on different functional groups. Sahiner and coworkers highlighted the catalytic efficiency of quaternized nitrogen groups, demonstrating their significant impact on hydrogen production in the methanolysis of $NaBH_4$ [3–9]. These studies demonstrated that quaternized nitrogen significantly increases the catalytic effect. Abebe et al. [10] investigated the role of carboxylic acids in hydrogen production. Ekinci et al. [11] emphasized that hydrochar interacts with the boron atom of borohydride and the oxygen atom of MeOH. Ma et al. [12] examined the functional groups present in natural lignin. In addition, Onat et al. (2024) reported Ru@CQDs catalysts for ammonia borane hydrolysis, achieving hydrogen generation rates exceeding 159,000 mL g^{-1} min^{-1}, though relying on noble metals and hydrolytic pathways [13]. Similarly, sucrose-derived Ru@CQDs catalysts have demonstrated very high HGR values in both $NaBH_4$ and KBH_4 hydrolysis (167,588 and 122,527 mL g^{-1} min^{-1}, respectively), further highlighting the strong performance of hydrolytic systems [14]. However, a review of the literature shows that studies on catalysts involving multiple interactions simultaneously (ion–dipole, ion–ion, hydrogen bonding, etc.) remain limited. Therefore, many factors should be considered simultaneously when designing a catalyst. Recently, metal-free catalysts derived from biomass and heteroatom-doped carbons have emerged as promising alternatives to conventional metal-based systems, showing high H_2 generation activity in $NaBH_4$ methanolysis [15, 16]. Recent reports have also emphasized environmentally friendly catalytic systems for $NaBH_4$ hydrolysis in different solvents, underscoring the versatility and strong activity of hydrolysis-based approaches [17]. In particular, phosphorus and oxygen co-doping of biomass-derived carbons has been shown to significantly enhance catalytic H_2 generation from $NaBH_4$ methanolysis, with Spirulina-based catalysts achieving HGR values up to 19,500 mL min^{-1} g^{-1} [18]. Similarly, oxygen and nitrogen co-doping on Spirulina-derived carbon nanoparticles resulted in a four-fold enhancement in catalytic activity, reaching HGR values of 10,105 mL min^{-1} g^{-1}, further highlighting the promise of heteroatom-enriched metal-free catalysts [19]. Nevertheless, methanolysis remains advantageous compared to hydrolysis, particularly in avoiding by-product accumulation and operating efficiently under milder conditions [18]. In this context, the rationale for selecting a zwitterionic polymer catalyst lies in its ability to combine cationic and anionic functionalities within the same macromolecular framework. This dual charge balance generates multiple complementary interaction sites that can simultaneously stabilize $NaBH_4$ and MeOH, thereby facilitating methanolysis through synergistic effects. Specifically, quaternized ammonium groups enhance electrostatic interactions with borohydride anions, while sulfonate groups promote ion–dipole and hydrogen–bonding interactions with methanol. In addition, ester moieties further strengthen hydrogen bonding, thereby collectively lowering the activation barrier. This synergistic functionality distinguishes zwitterionic polymers from conventional single-function catalysts and highlights their potential for enhanced hydrogen generation activity.

In addition to their chemical functionality, the environmental impact of catalysts is a critical factor to consider. Traditional catalysts are mostly based on metals and metal alloys, which are effective but costly and environmentally harmful [10, 20–22]. Because they are difficult to dispose of after use, they cause serious environmental problems. In this context, poly(2-diethylaminoethyl methacrylate) (PDMA) has emerged as a promising alternative. PDMA is a water-soluble polymer containing tertiary amino groups, which can be easily protonated in acidic media. Due to its biocompatibility and pH- and heat-sensitive nature, it

is generally used to prepare materials for controlled drug-delivery systems [23, 24], and contact lenses perez talanta [24]. As a result, (i) its biocompatibility, (ii) its ability to adopt cationic and anionic structures with simple modifications, and (iii) its hydrogen-bonding groups such as esters demonstrate that PDMA is an important alternative catalyst for $NaBH_4$ methanolysis reactions. However, to the best of our knowledge, no study has reported hydrogen production using zwitterionic polymers derived from P(DMA).

Building on these insights, the aim of this study is to present an innovative approach to catalyst design and to synthesize more effective and environmentally friendly catalysts using this strategy. P(Q-DMA), synthesized by modifying 2-(dimethylamino)ethyl methacrylate (DMA) with 1,3-propanesultone (PS) followed by polymerization, was designed to exhibit ion–dipole, ion–ion, and hydrogen-bonding interactions. Experimental results demonstrated that P(Q-DMA) significantly outperformed conventional catalysts in terms of catalytic efficiency and environmental compatibility. This pioneering approach provides a foundation for future advances in catalyst design for renewable energy applications, particularly hydrogen production. The insights gained from this study may guide the development of next-generation polymeric catalysts with enhanced performance and scalability, potentially transforming industrial processes for sustainable energy systems. Although zwitterionic polymers have previously been reported in electrochemical and biomedical applications, to the best of our knowledge, their direct catalytic potential in sodium borohydride methanolysis has not been systematically investigated. This study addresses this gap by integrating zwitterionic functionality into a polymeric catalytic network, offering new insights into structure–activity relationships in metal-free systems. By correlating kinetic parameters (e.g., activation energy, Eyring analysis) with surface characteristics and functional groups, this work contributes to both fundamental catalysis research and practical hydrogen-generation applications.

2 Material and Methods

2.1 Materials

2-(Dimethylamino)ethyl methacrylate (DMA, $C_7H_{13}NO_2$, 98%, Sigma-Aldrich), 1,3-propanesultone (PS, $C_3H_6O_3S$, 98%, Sigma-Aldrich), ethylene glycol dimethacrylate (EGDMA, $C_{10}H_{14}O_4$, 98%, Sigma-Aldrich), 2,2′-azobis(2-methylpropionitrile) (AIBN, $C_8H_{12}N_4$, 98%, Sigma-Aldrich), tetrahydrofuran (THF, C_4H_8O, anhydrous, ≥ 99.9%, Sigma-Aldrich), and methanol (MeOH, CH_3OH, ≥ 99.8%, Merck) were used in this study. Before use, DMA was purified by passing through a silica column, and AIBN was recrystallized in MeOH. All other chemicals were used as received without further purification. Deionized water (18.2 MΩ·cm, Millipore system) was used throughout the experiments.

2.2 Quaternization of DMA

The quarternization of DMA was synthesized according to [25, 26]. Briefly, 100 mL of dry THF was added to the round-bottomed reaction flask, closed with a septum, and degassed with N_2 gas for 20 min. Then, 10 mL (59.35 mmol) of freshly DMA monomer, passed through a silica column, was added to this flask with a syringe and degassing continued. Meanwhile, certain amounts of dry THF and 7.24 g (59.35 mmol) of PS were added to another vial, closed with a septum, and degassed with N_2 gas. After 30 min, the PS solution was added dropwise to the DMA solution with a cannula. The DMA solution began to become cloudy while the PS solution was added. The reaction was continued overnight at room temperature. At the end of the reaction, the milky white precipitate was decanted and washed several times with THF to remove impurities. Finally, the sulfobetaine DMA (Q-DMA) monomer was filtered and dried in a freeze dryer (Fig. 1A).

2.3 Polymerization of Q-DMA

For polymerization, in a round-bottomed reaction flask, 2 g (8.1 mmol) of Q-DMA was dissolved in 12 mL of pure water and then certain amount of dry THF (until the solution started to become cloudy) and then 2.5 mol% EGDMA were slowly added. Meanwhile, 50 µg of AIBN and 2 mL dry THF were added to a separate vial, respectively. Both solutions were closed with a septum and degassed with N_2 gas for 20 min. Q-DMA solution was heated to 65 °C and then the AIBN solution was added. The reaction was continued overnight. At the end of the reaction, the polymer precipitate was filtered, and washed several times with distilled water and THF and dried in a freeze dryer (Fig. 1B).

2.4 Characterization of P(Q-DMA) Polymers

The P(Q-DMA) polymers were analyzed using various techniques to determine their properties. Morphological analysis was performed by scanning electron microscopy (SEM) by using an FEI Quanta FEG250 device. Functional groups within the polymer were identified by FT-IR spectroscopy using a Bruker Alpha model instrument, which recorded spectra with a resolution of 4 cm-1 in the 4000–500 cm-1 range. Thermal stability was evaluated using a Tetra SII Exster 6000 instrument under a nitrogen atmosphere, heating samples from 25 °C to 1000 °C at 5 °C/min. Surface

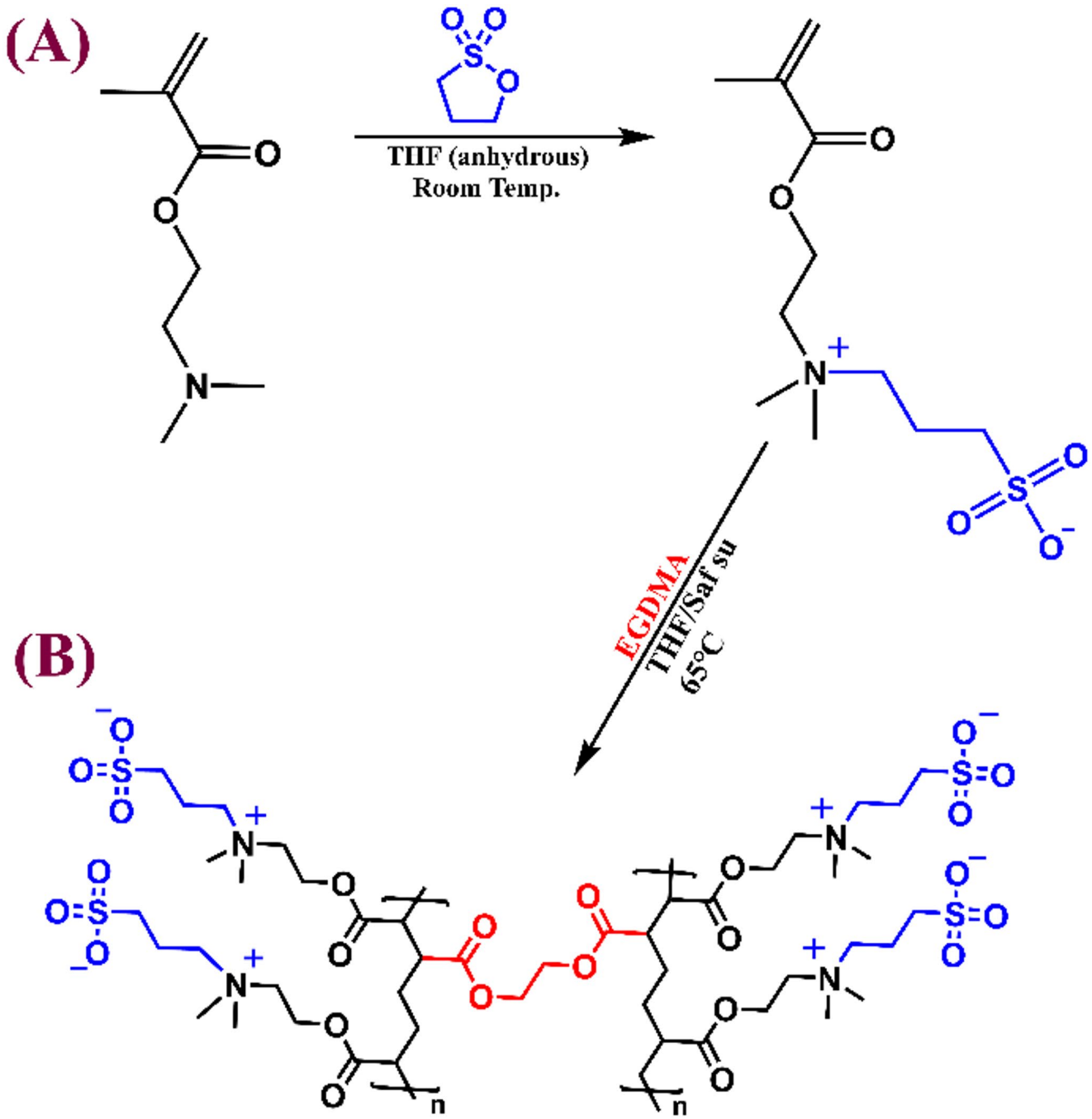

Fig. 1 Betainisation of DMA **(A)** and polymerization of Q-DMA **(B)**

area and porosity were evaluated using a Quantachrome Nova Touch LX4. Zeta potential measurements were performed with a Zetasizer Nano ZS (Malvern Instruments) to determine the surface charge of the catalysts before and after $NaBH_4$ methanolysis.

2.5 Hydrogen Generation Tests

The catalytic performance of P(Q-DMA) in $NaBH_4$ methanolysis was evaluated using a water displacement method to measure hydrogen evolution. Experiments were conducted using 50 mg P(Q-DMA), 125 mg $NaBH_4$ in 10 mL MeOH under stirring at 750 rpm and 30 °C. In addition, optimization studies were carried out to further elucidate the catalytic effect of P(Q-DMA). In these studies, the optimum amounts

of P(Q-DMA) (25–250 mg) and $NaBH_4$ (50–150 mg), volume of MeOH (2–10 mL) and temperature (25–60 °C) on hydrogen production were determined. Activation energy (Ea), activation enthalpy ($\Delta H^{\#}$), and activation entropy ($\Delta S^{\#}$) were calculated using Arrhenius and Eyring equations based on temperature-dependent data.

2.6 Electrochemical Measurements

The catalytic activity of the polymer for $NaBH_4$ electrooxidation was determined by electrochemical measurements performed on a CHI 660E potentiostat device. Experimental measurements were performed with a 3-electrode system consisting of a glassy carbon electrode as the working electrode, Ag/AgCl electrode as the reference electrode, and platinum wire as the counter electrode. CV measurements were taken in 1 M NaOH and 1.0 M NaOH + 0.1 M $NaBH_4$ solutions and the electrocatalytic activity of the polymer was determined. The stability and catalytic resistance of the polymer were evaluated by CA and EIS measurements at different voltage values, respectively.

2.7 Computational Methods

Density Functional Theory Calculations using B3LYP functional were used with a basis set containing polarization and diffuse functions at 6–311+g(d) level was used in calculations using Gaussian 16, Revision C.02 [27, 28]. D3 dispersion correction by Grimme was applied in all calculations [29]. All calculations were performed in implicit methanol solvent effect by using IEFPCM method [30]. Interaction energies were calculated for the lowest energy structures by using counterpoise method for BSSE correction [31].

3 Results and Discussions

3.1 Characterization of Catalysts

The proton NMR spectrum of the compound Q-DMA revealed key structural insights, confirming successful quaternization (Fig. 2). The spectrum showed vicinal and geminal vinyl protons at 6.00 ppm and 5.62 ppm, respectively. Four methylene (-CH_2-) groups, each adjacent to a

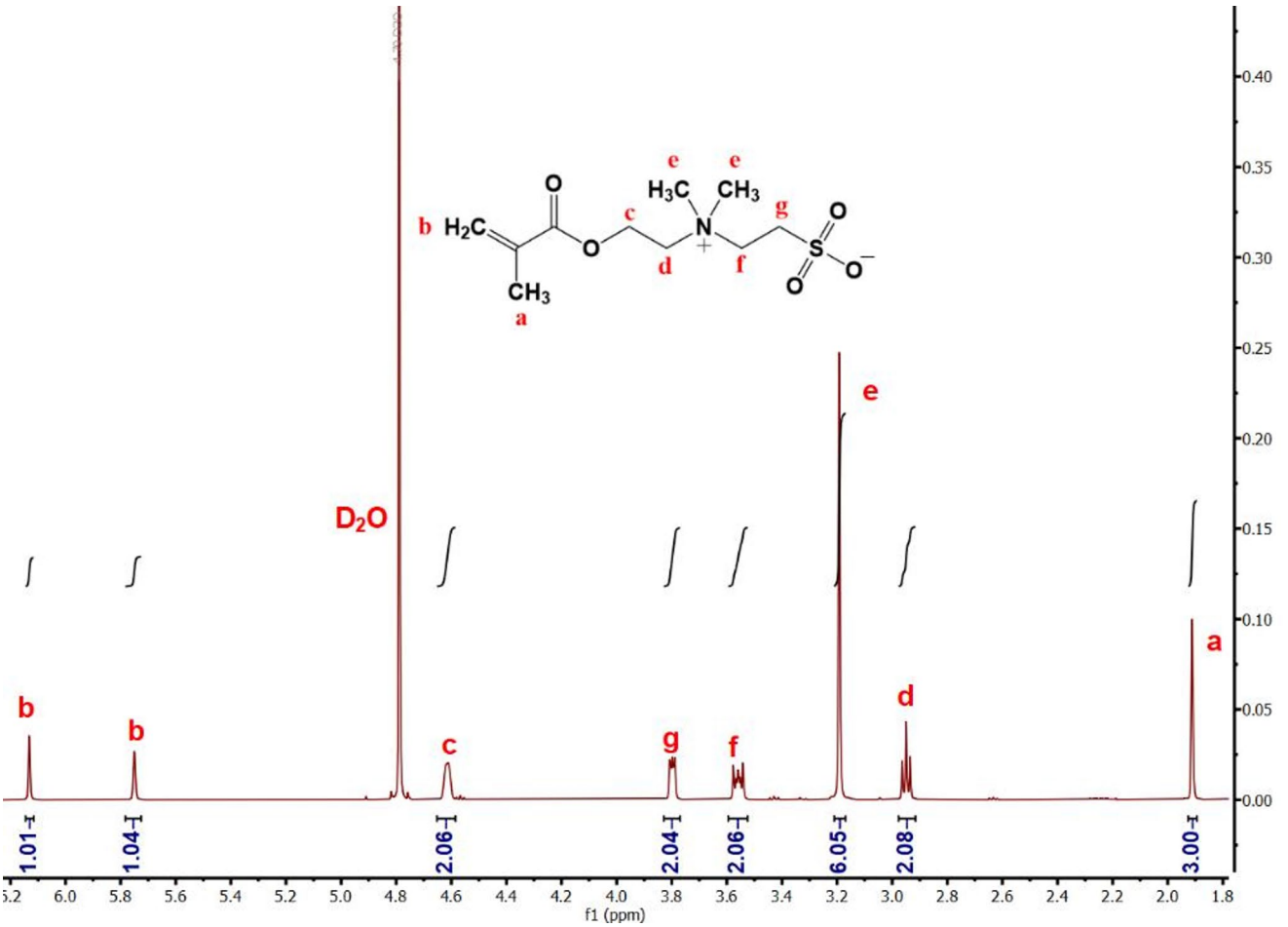

Fig. 2 ^{1}H NMR spectrum of Q-DMA monomer

carbon atom with two hydrogen atoms, were identified as triplets with chemical shifts at 4.66 ppm (H_c), 3.43 ppm (H_d), 3.66 ppm (H_f), and 4.48 ppm (H_g). The two methyl protons attached to the quaternary nitrogen group resonated at 3.06 ppm, while the methyl group of the methacrylate moiety was observed at 1.78 ppm. The integration of all signals matched the theoretical proton count, validating the successful synthesis of the target compound.

The P(Q-DMA) structure was confirmed through Fourier Transform Infrared (FT-IR) spectroscopy, as illustrated in Fig. 3. The spectrum was recorded with a resolution of 4 cm^{-1} in the range of 4000–500 cm^{-1}, clearly displaying characteristic peaks corresponding to functional groups in the polymer. The aliphatic –C–H stretching vibrations were observed between 3000 and 2800 cm^{-1}, accompanied by C–H scissoring bands at 1477 cm^{-1}. The ester group exhibited distinct signals at 1722 cm^{-1} for C=O stretching and at 1033 cm^{-1} for C–O stretching. Furthermore, the quaternary ammonium group ($R_2NH_2^+$) showed N–H bending at 1645 cm^{-1} and N–H stretching at 3417 cm^{-1}. The sulfate group ($–SO_3^-$) presented strong absorption bands at 1163 cm^{-1} for S=O stretching and 601 cm^{-1} for S–O stretching. These peaks collectively confirm the successful formation and chemical modification of P(Q-DMA), highlighting its readiness for catalytic applications.

SEM images (20–2 µm) of P(Q-DMA) polymer are presented in Fig. 4. When the images were examined, it was understood that P(Q-DMA) polymer was synthesized as irregular particles. The sizes of the 100 particles in Fig. 4B were calculated with ImageJ software (excluding very large particles). Accordingly, the average particle size of P(Q-DMA) was determined as 1180 mn, and the sizes of the smallest and largest particles were determined as 540 and 2641 nm, respectively.

Thermogravimetric Analysis (TGA) results highlight the thermal stability of P(Q-DMA, Fig. 5). An initial mass loss

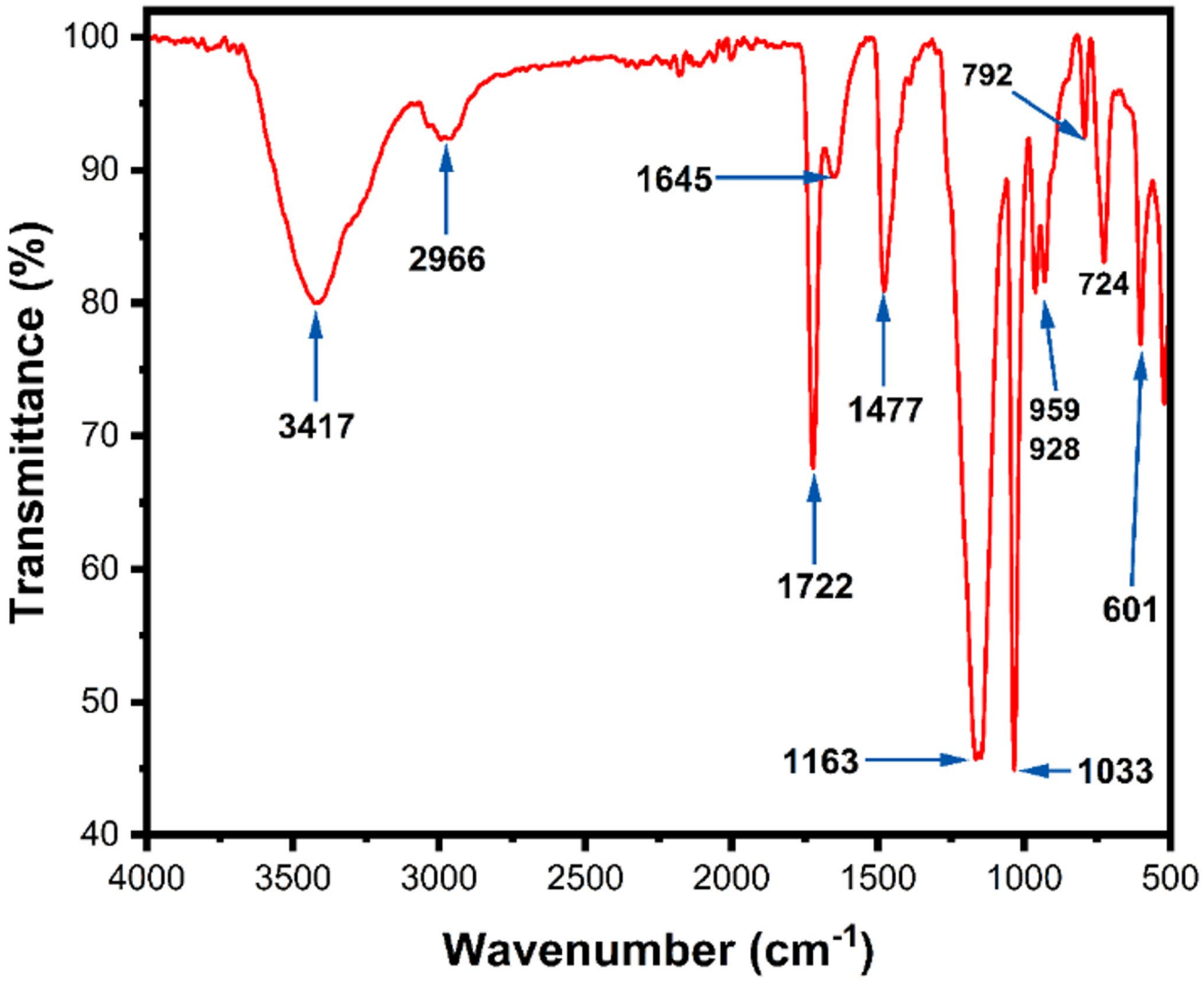

Fig. 3 FT-IR spectrum of P(Q-DMA)

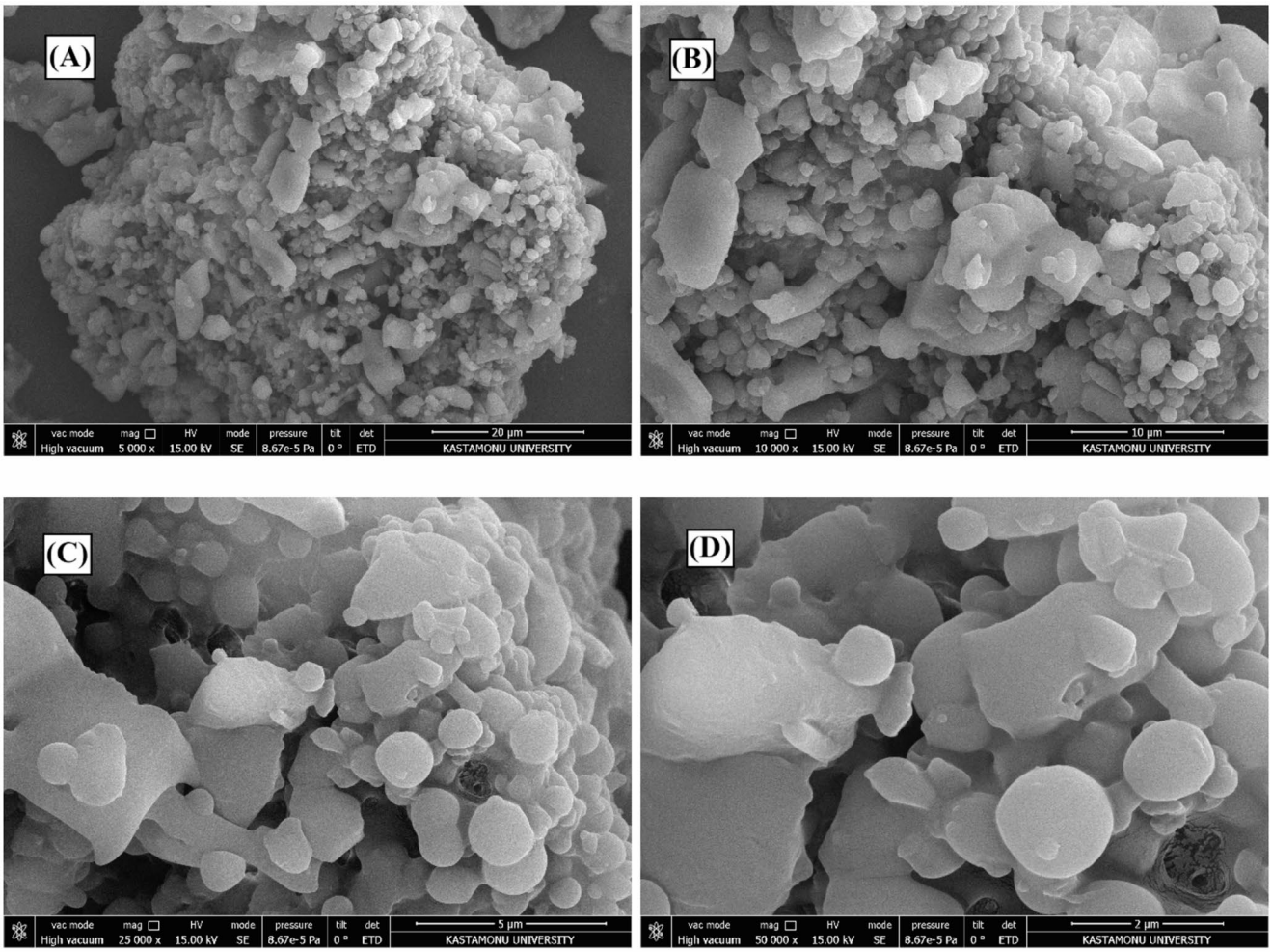

Fig. 4 SEM micrographs of P(Q-DMA) polymer with different scale bars (**A**: 20 µm, **B**: 10 µm, **C**: 5 µm, **D**: 2 µm)

of 11.88 wt% below 130 °C corresponds to the evaporation of solvents and/or volatile compounds embedded within the polymer matrix. Degradation occurs in two main stages, with significant weight losses of 53.18 wt% at 365 °C and 25.31 wt% at 450 °C. At 800 °C, the residual mass was found to be 4.42 wt%, indicating excellent thermal stability suitable for catalytic applications.

3.2 Hydrogen Generation Results

3.2.1 Effect of Methanol Volume on $NaBH_4$ Methanolysis

The effect of MeOH volume on hydrogen production via $NaBH_4$ methanolysis was systematically evaluated under various conditions. Experiments were conducted with MeOH volumes of 2, 4, 6, 8, and 10 mL, keeping other parameters constant: 50 mg of P(Q-DMA) catalyst, 125 mg $NaBH_4$, 30 °C, and a stirring speed of 750 rpm. The required volume of hydrogen was successfully produced in all experiments. The results obtained are given in Fig. 6. As can be seen from Fig. 6A, the required hydrogen volume for 2, 4, 6, 8 and 10 mL MeOH was produced in 3, 2.25, 2.5, 2.25 and 2 min, respectively. HGR values were calculated as 5826.96, 7996.08, 7164.84, 7941.24 and 8868.36 mL H_2 min^{-1} g_{cat}^{-1}, respectively (Fig. 6B). The increase in HGR with higher MeOH volumes can be attributed to the enhanced solvation of NaBH4, facilitating its decomposition and subsequent hydrogen release. However, it was observed that additional MeOH did not significantly reduce reaction time beyond a certain point (10 mL). This plateau effect suggests that an optimal solvent-to-reactant ratio exists for maximizing the efficiency of NaBH4 methanolysis. Previous studies reported comparable trends, such as those involving Co/activated carbon (Co/AC) catalysts, where higher MeOH volumes similarly led to improved hydrogen production rates [32]. For example, Sahiner et al. reported HGR values of 6783.12, 6798.84, and 9432.72 mL H_2 min^{-1} $gcat^{-1}$ for 2, 4, and 6 mL MeOH, respectively. The slightly higher efficiency of P(Q-DMA) can be attributed to its zwitterionic structure, which promotes stronger

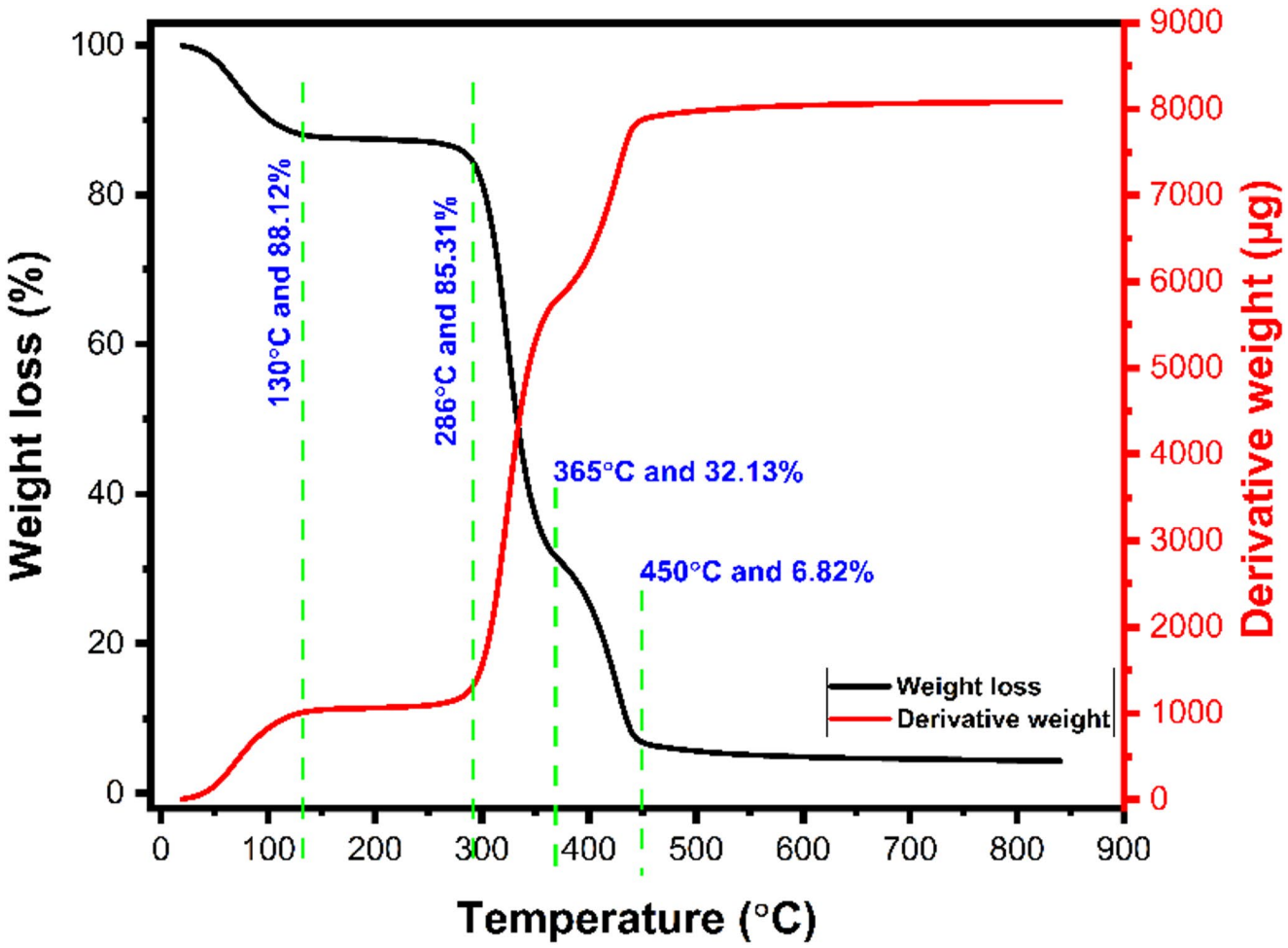

Fig. 5 Thermogravimetric analysis of P(Q-DMA)

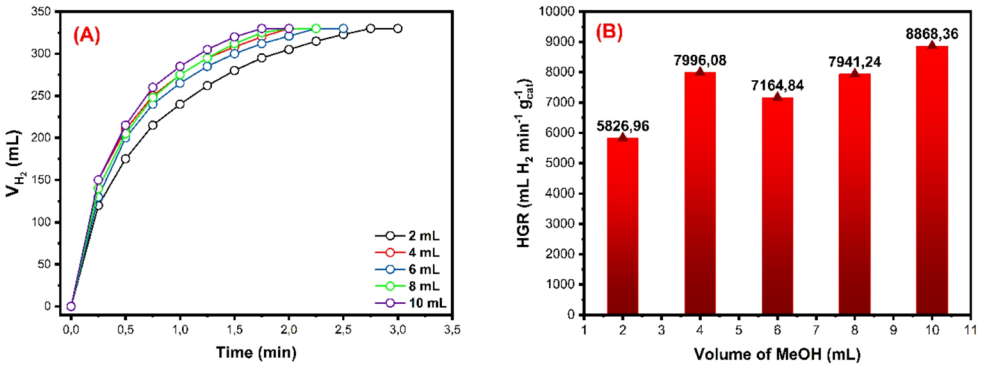

Fig. 6 Effect of MeOH volume on (**A**) H_2 production and (**B**) HGR values of P(Q-DMA) (Reaction conditions: 50 mg P(Q-DMA), 0.100 g $NaBH_4$, 20 mL MeOH, 298 K, stirring rate 750 rpm)

ion–dipole and hydrogen-bonding interactions. Identifying 10 mL as the optimal MeOH volume underscores the importance of solvent selection and optimization in catalytic hydrogen production systems. These results highlight the superior catalytic efficiency of P(Q-DMA) and provide valuable insights into the mechanistic role of methanol in facilitating $NaBH_4$ methanolysis. Identifying 10 mL as the optimal methanol volume provides a basis for scaling up the reaction for industrial hydrogen production. Further studies could explore methanol recovery and recycling systems to enhance the sustainability of this process.

3.2.2 Effect of P(Q-DMA) Amounts on $NaBH_4$ Methanolysis

Determining the optimal amount of catalyst is quite significant for balancing efficiency and cost-effectiveness in hydrogen production. Therefore, determining the optimum catalyst amount is critical. To evaluate the optimal catalyst

loading, experiments were conducted using 25, 50, 125, and 250 mg of P(Q-DMA), while keeping other parameters constant (10 mL MeOH, 125 mg $NaBH_4$, 30 °C, 750 rpm). The results are summarized in Fig. 7. Accordingly, the required hydrogen volume for 25, 50, 125 and 250 mg P(Q-DMA) was produced in 3.75, 2, 2.5 and 2 min, respectively (Fig. 7A). As for the HGR values, the required hydrogen volume for 25 mg P(Q-DMA) amount was produced at least 1.5 times longer than other P(Q-DMA) amounts. The difference between the production times for other amounts was negligible. The reaction rates for 25, 50, 125 and 250 mg P(Q-DMA) amounts were calculated as 252.57, 443.42, 367.34 and 455.28 mL H_2 min^{-1} and the HGR values were calculated as 10,102.8, 8868.36, 2938.75 and 1821.1 mL H_2 $min^{-1}g_{cat}^{-1}$, respectively (Fig. 7B). The number of active sites that exhibit catalytic effect increases with the increase in the amount of catalyst. As a result, the reaction rate also increases [33, 34]. The obtained results proved also this phenomenon. However, the observed decline in HGR beyond 50 mg suggests that excessive catalyst amount may lead to aggregation of the polymers, reducing the accessibility of active sites. This phenomenon underscores the importance of balancing catalyst quantity to achieve efficiency and cost-effectiveness. Similar results were obtained for P(2-VP) supported Ru(II) used as a catalyst in the production of hydrogen by methanolysis of $NaBH_4$ [35]. For example, the reaction rates and HGR values for 10, 25, 50 and 100 mg catalyst amounts were determined to be 149, 148, 167 and 170 mL H_2 min^{-1} and 2980, 1192, 669 and 339 mL H_2 $min^{-1}g_{cat}^{-1}$, respectively in that study. Hydrogen production times were reported to be around 5 min. These findings confirm the significant role of catalyst amount in optimizing hydrogen production efficiency [35].

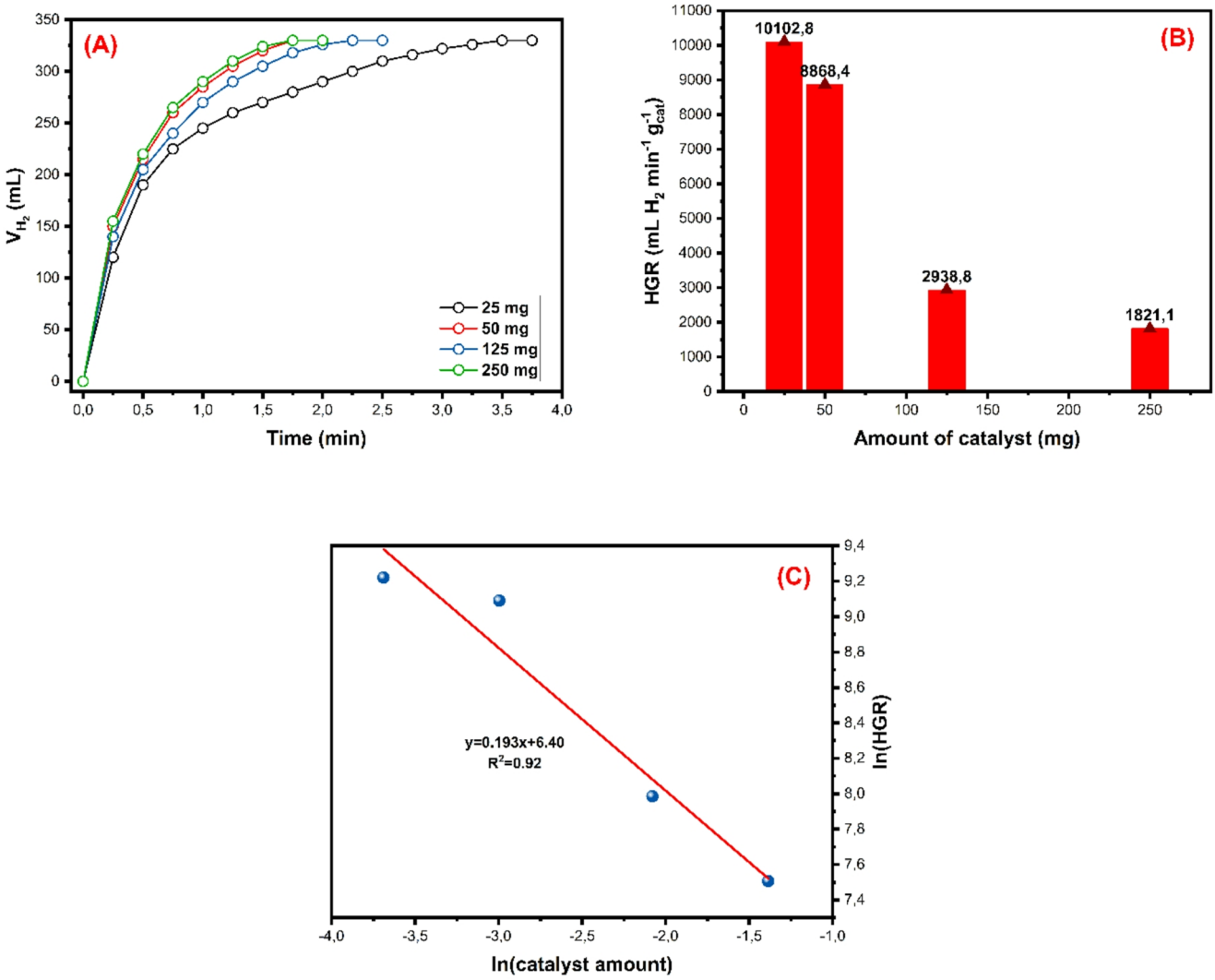

Fig. 7 (**A**) Effect of P(Q-DMA) amount on hydrogen production, (**B**) corresponding HGR values of P(Q-DMA), and (**C**) reaction kinetics of P(Q-DMA) (Reaction conditions: 10–60 mg P(Q-DMA), 0.125 g $NaBH_4$, 10 mL MeOH, 298 K, stirring rate 750 rpm)

In this study, the kinetics of the reaction was also investigated with the graph drawn with ln(*catalyst amount*) and ln(*HGR*) (Fig. 7C). The slope (0.193) of this graph showed that it was a zero-order reaction according to the amount of P(Q-DMA). Hydrogen production times for 25 and 50 mg P(Q-DMA) were found to be 3.75 and 2 min, respectively, and HGR values were found to be 10,102.8 and 8868.36 mL H_2 $min^{-1}g_{cat}^{-1}$. Although the HGR value obtained with 25 mg P(Q-DMA) was higher, the hydrogen production time was 1.88 times slower. In addition, the HGR values obtained for 25 and 50 mg P(Q-DMA) were quite close to each other. Therefore, hydrogen production times were decisive in determining the appropriate catalyst amount and the following experiments were continued with the amount of 50 mg P(Q-DMA). Identifying 50 mg as the optimal catalyst amount provides critical insights into the efficient utilization of P(Q-DMA). This finding emphasizes the polymer's superior catalytic performance and aligns with sustainable practices by minimizing material usage without compromising efficiency. Future work could explore scaling these findings for industrial applications, ensuring larger-scale cost-effectiveness.

3.2.3 Effect of $NaBH_4$ Amounts on $NaBH_4$ Methanolysis

In this study, the effect of the amount of $NaBH_4$ on hydrogen production was systematically investigated. For this purpose, experiments were conducted with 50, 100, 125 and 150 mg $NaBH_4$ amounts, while 10 mL MeOH, 50 mg P(Q-DMA), 30 °C and 750 rpm stirring speed were kept constant. The findings are presented in Fig. 8. Accordingly, the required hydrogen volume for 50, 100, 125 and 150 mg $NaBH_4$ amounts was produced in 1.5, 2, 2 and 2.25 min, respectively (Fig. 8A). The reaction rates were calculated as 243.01, 346.90, 443.42 and 467.57 mL H_2 min^{-1} and HGR values were calculated as 4860.12, 6937.92, 8868.36 and 9351.48 mL H_2 $min^{-1}g_{cat}^{-1}$, respectively (Fig. 8B). Accordingly, with the increase in the amount of $NaBH_4$, both the reaction rate and HGR increased. The increase in HGR with higher $NaBH_4$ amounts can be attributed to the greater availability of borohydride ions, which enhances the rate of methanolysis. The linear effect in the reaction rate and HGR with the increase in the amount of $NaBH_4$ was also reported by Sahiner [4]. In that study, it was found that when the amount of $NaBH_4$ was increased from 62.5 mM to 400 mM, the HGR value increased from 1422 to 7710 mL H_2 $min^{-1}g_{cat}^{-1}$, respectively. A similar effect was also seen in the studies conducted by Inger et al. [36] and Dudu et al. [21].

The effect of $NaBH_4$ amount on the reaction kinetics was also investigated with the logarithmic values of the amount of $NaBH_4$ and HGR values in this study (Fig. 8C). The slope of this graph was calculated as 0.386. Accordingly, it was understood that the reaction kinetics was of the zero degree according to the amount of $NaBH_4$. According to these results, it was decided that the amount of 125 mg $NaBH_4$ was appropriate. This amount was kept constant in the following experiments. Another factor in choosing this amount of $NaBH_4$ was that the data obtained could be compared accurately with the literature, because a significant portion of the data reported in the literature was obtained with 125 mg $NaBH_4$.

These results underscore the importance of optimizing $NaBH_4$ concentration for efficient hydrogen production. The ability of P(Q-DMA) to achieve high HGR even at moderate $NaBH_4$ concentrations highlights its potential for scalable and cost-effective applications in hydrogen energy systems.

3.2.4 Effect of Temperature on $NaBH_4$ Methanolysis

Temperature is also one of the most effective parameters for the hydrogen production as in all reactions. Therefore, experiments were carried out with different temperatures (25, 30, 40, 50 and 60 °C) to elucidate the hydrogen production and the capacity of the catalyst, while 10 mL MeOH, 50 mg P(Q-DMA), 125 mg NaBH4 amount and 750 rpm stirring speed were kept constant. The results are summarized in Fig. 9. Accordingly, the hydrogen production times for 25, 30, 40, 50 and 60 °C temperatures were 2, 2, 1.75, 1.25 and 1.25 min, respectively (Fig. 9A). The reaction rates were calculated as 435.88, 434.39, 535.99, 771.68 and 837.90 mL H_2 min^{-1} and HGR values were 8717.52, 8787.84, 10,719.84, 15,433.60 and 16,758 mL H_2 $min^{-1}g_{cat}^{-1}$, respectively (Fig. 9B). As expected, the catalytic performance of P(Q-DMA) increased in all aspects with the increase in temperature. Similar temperature-dependent trends were observed with other catalysts. Similar results were reported for poly(acrylic acid)-modified silica nanoparticles [10]. HGR values increased from 5120 to 12,211 mL H_2 $min^{-1}g_{cat}^{-1}$ when the temperature was increased from 20 °C to 50 °C in that study. This high effect of temperature was also revealed in other studies [4, 37–41].

This study highlighted the importance of both P(Q-DMA) and $NaBH_4$ amount, and temperature in optimizing hydrogen production via $NaBH_4$ methanolysis. The observed reaction kinetics emphasized the importance of these parameters in achieving efficient hydrogen production. Optimizing reaction temperature is crucial for maximizing efficiency in catalytic hydrogen production. The superior performance of P(Q-DMA) across a wide temperature range demonstrates its robustness and versatility, reinforcing its potential for industrial applications. Future studies could explore the integration of heat recovery systems to mitigate

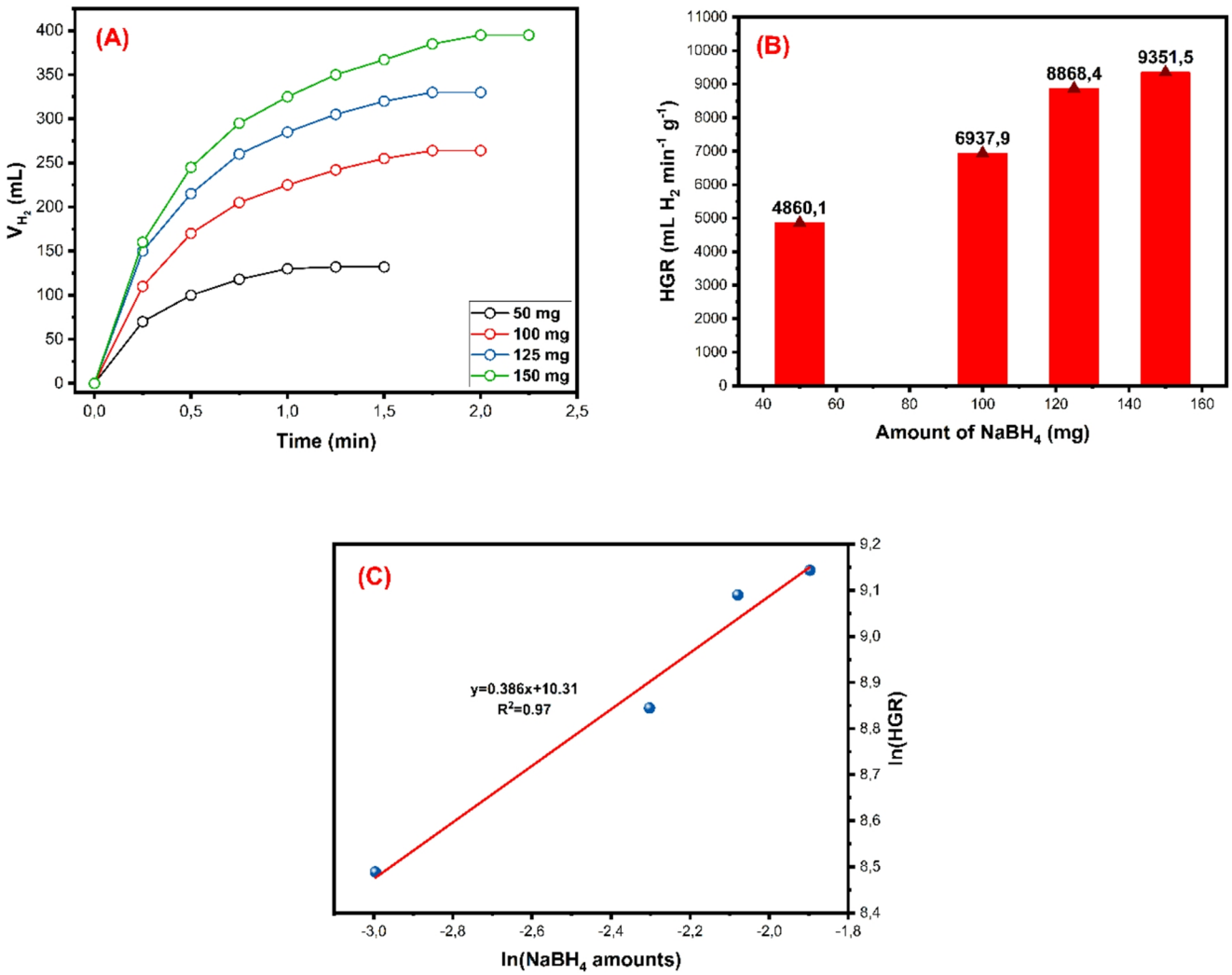

Fig. 8 Effect of the amount of $NaBH_4$ in hydrogen production **(A)**, HGR values of P(Q-DMA) **(B)**, and reaction kinetics of P(Q-DMA) **(C)**. (Reaction conditions: 50 mg P(Q-DMA), 0.05–0.20 g $NaBH_4$, 10 mL MeOH, 298 K, stirring rate 750 rpm)

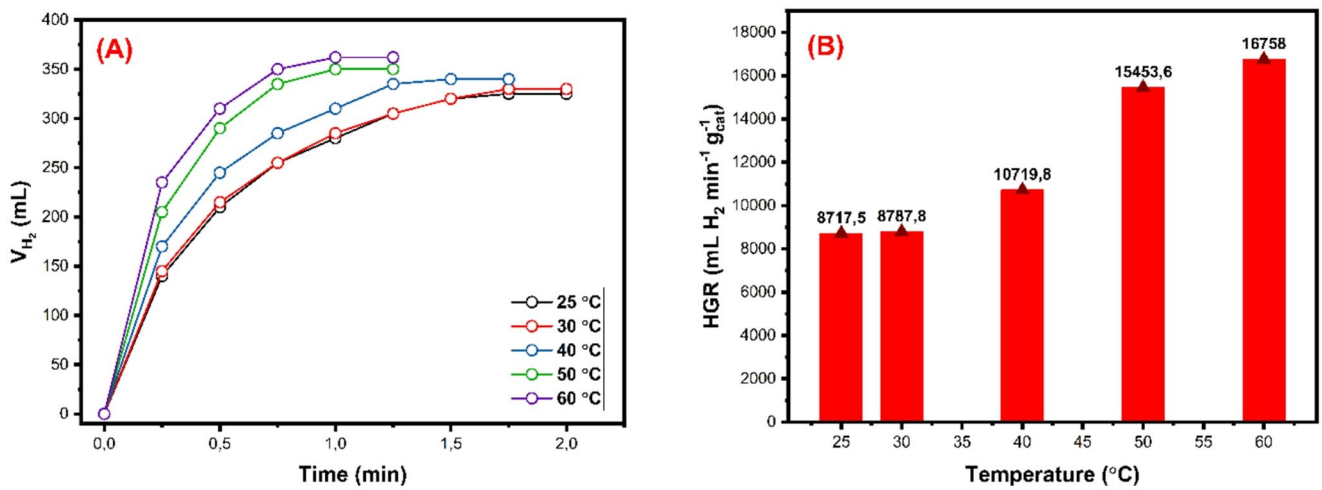

Fig. 9 (**A**) Effect of temperature on hydrogen production and (**B**) corresponding HGR values of P(Q-DMA) (Reaction conditions: 50 mg P(Q-DMA), 0.125 g $NaBH_4$, 10 mL MeOH, temperature range 0–60 °C, stirring rate 750 rpm)

energy costs and further enhance the sustainability of this process. The results emphasize optimizing reaction temperature to maximize efficiency while minimizing energy costs. Future studies could integrate heat recovery systems to mitigate the energy requirements of high-temperature operations, enhancing the overall economic feasibility.

To further understand the temperature dependence of hydrogen production, the activation energy (Ea) for P(Q-DMA) was calculated using the Arrhenius equation Eqs. (1) and (2):

$$k = A.e^{-Ea/RT} \quad (1)$$

$$\ln k = \ln A - E_a/RT \quad (2)$$

In the equations, k is the reaction rate constant, A is the Arrhenius constant, R is the ideal gas constant, T is the temperature and E_a is the activation energy. The plot of 1/T *versus* lnk is shown in Fig. 10A. The activation energy was calculated from the slope of this graph. Accordingly, the activation energy of P(Q-DMA) was determined to be 19.91 kJ mol^{-1}. When comparing the results, the activation energy of P(Q-DMA) was found to be quite favorable compared to the literature (Table 2). For instance, natural lignin-based catalysts exhibited E_a values of 19.5 kJ mol^{-1}, while TD particles (ATIF 38) catalysts demonstrated E_a values as low as 16.86 kJ mol^{-1}. Compared to these, P(Q-DMA) provides a competitive advantage due to its high HGR values coupled with low E_a, making it a highly efficient and scalable option.

Additionally, using Fig. 10B which was drawn using the Eyring equation given in Eq. 3, $\Delta H^{\#}$ (activation enthalpy) and $\Delta S^{\#}$ (activation entropy) values were calculated as 17.27 kJ mol^{-1} and −185.57 kJ mol^{-1}, respectively, while $\Delta G^{\#}$ were found as 56,27 kJ mol^{-1}.

$$\ln\frac{k}{T} = -\frac{\Delta H^{\#}}{R}\frac{1}{T} + \ln\frac{k_B}{h} + \frac{\Delta S^{\#}}{R} \quad (3)$$

In this equation, k_B is the Boltzmann constant (1.381×10^{-23} J K^{-1}), h is Planck constant (6.626×10^{-34} J.s).

3.2.5 Catalytic Mechanism Between P(Q-DMA), $NaBH_4$, and MeOH

An ideal catalyst for the methanolysis of $NaBH_4$ should strongly interact with $NaBH_4$ and MeOH through adsorption processes. $NaBH_4$ has BH_4^- anion in its structure and its hydrogens are nucleophile. The BH_4^- anion interacts with the cations in the medium either ion-ion and/or ion–dipole or hydrogen bonds with molecules with polar molecules and heteroatoms. On the other hand, MeOH has a dipole moment due to the high electronegativity of the oxygen in its structure. Thanks to this feature, MeOH shows ion–dipole interaction with the ions in the medium and makes hydrogen bonds with the hydrogen in its structure with heteroatoms. Therefore, the simultaneous presence of ions and heteroatoms that can enter strong ion-ion and/or ion–dipole and hydrogen bond interactions in the structure of a catalyst are the most important features that will determine the catalytic effect of that catalyst. In other words, the number of ions and heteroatoms determines the performance of a catalyst and decreases the activation energy of the reaction. Although the surface area and pore volume of the catalyst are also important in this interaction, this study focused only on the effects of ion-ion, ion–dipole and hydrogen bonds. For this purpose, P(Q-DMA) which is biocompatible and has a zwitterion structure was used for the first time in the production of hydrogen from $NaBH_4$ by methanolysis. P(Q-DMA) contains quaternized nitrogen (cationic) and sulfonate groups (anionic). In addition,

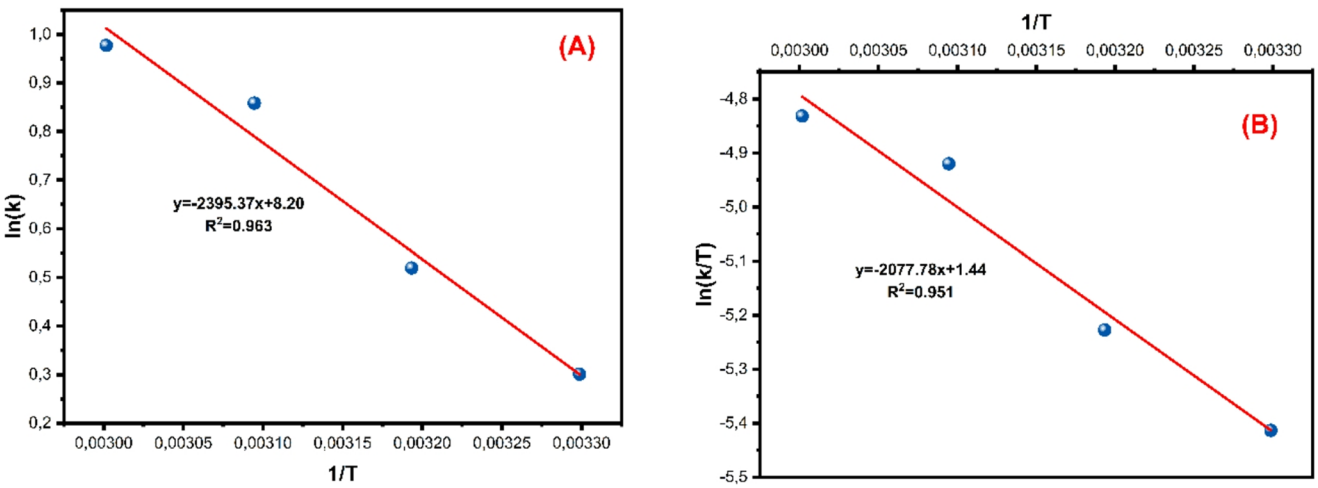

Fig. 10 (**A**) Arrhenius plot of 1/T vs ln k and (**B**) Eyring plot of 1/T vs ln (k/T) for $NaBH_4$ methanolysis catalyzed by P(Q-DMA) (Reaction conditions: 0–60 °C, 50 mg P(Q-DMA), 0.125 g $NaBH_4$, 10 mL MeOH, stirring rate 750 rpm)

Table 1 Comparing of HGR and E_a values of various catalysts for $NaBH_4$ methanolysis in other studies

Catalyst	Temp (°C)	HGR (mL H_2. min^{-1})	HGR (mL $H_2.min^{-1}g_{cat}^{-1}$)	E_a (kJ mol^{-1})	Method	Ref.
Carbon nanotube (CNT) supported bimetallic CuBi catalysts	30	485.8	9716.3	34.72	Methanolysis	[37]
Co/activated carbon (Co/AC)	30	344.7	6895.08	11.29	Methanolysis	[25]
PdNi@VC NPs	30	-	2727.4	54.2	Methanolysis	[40]
P(AEM)-Co	30	-	842	38.2	Hydrolysis	[10]
P(AEM)			236	42.5	Methanolysis	
$P(AEM)^+Cl^-$			1366	37.3	Methanolysis	
TD particles	30	549	21,960.2	16.86	Methanolysis	[4]
GD particles		394.6	39,459.6	18.14		
Natural lignin	25	1021.2	20,425	19.5	Methanolysis	[13]
Waste ceramic frit	30				Methanolysis	[36]
F1		501.35	10,027	18.21		
F2		441.9	8839	29.71		
AAPC-WBTL	50	76.76	7676	47.06	Methanolysis	[38]
AAPC-WGTL		90.85	9084.75	47.89		
Poly(2-vinyl pyridine)-hexane	30	271.7	5433	20.84	Methanolysis	[3]
P(AMPS)-TDA-1 PIL microgel	30	128.1	854	14.30	Methanolysis	[9]
$P(C_6VImBr)$ microgels	30	58.71	5871	34.30	Methanolysis	[5]
Chitosan coated cellulose cotton fibers	22	388	7760	14.41	Methanolysis	[39]
PDMA cryobeads	30	76.36	3818	19.34	Methanolysis	[41]
P(Q-DMA)	**30**	**443.4**	**8868.36**	**19.91**	**Methanolysis**	**This study**

sulfonate groups can make hydrogen bonds with the oxygens in their structure. Apart from this, it is well known that esters also make strong hydrogen bonds. Accordingly, since borohydride is anionic, it enters into electrostatic interaction with the quaternized nitrogen in the structure of P(Q-DMA) during the reaction. Meanwhile, the hydrogens of the borohydride form hydrogen bonds with the ester groups of P(Q-DMA). MeOH shows predominantly ion–dipole interaction with the anionic sulfonate group. Similar to the synergistic role of phosphorus and oxygen functionalities in carbon-based catalysts, which enhance electron transfer and adsorption capacity, the zwitterionic groups of P(Q-DMA) provide multiple complementary sites for efficient $NaBH_4$ methanolysis [42]. Also, compared to the reported oxygen/nitrogen doped microalgae-derived catalysts (Ea = 39.75 kJ mol^{-1}, HGR = 10,105 mL min^{-1} g^{-1}), our zwitterionic P(Q-DMA) system achieved a much lower Ea (19.91 kJ mol^{-1}) while maintaining competitive hydrogen generation performance [19].

It is also thought that hydrogen bonds are formed, albeit slightly, with the hydrogen in MeOH and the oxygens in the sulfonate group (in S=O) (Fig. 11). The catalytic mechanism can be summarized as follows;ds are formed, albeit slightly, with the hy

1. BH_4^- anion and MeOH entered into ion-ion and ion–dipole interactions with the quaternized nitrogen and anionic sulfonate groups in the structure of P(Q-DMA), respectively.
2. Concurrently, BH_4^- and/or MeOH formed hydrogen bonds with the ester group of P(Q-DMA).
3. MeOH attacked the boron atom of BH_4^-, while the nucleophilic hydrogen of BH_4^- racts the hydrogen of MeOH to produce H_2 gas.

Zeta potential measurements before and after methanolysis provided additional insights into the catalytic mechanism. The surface charge shifted from + 13.1 mV (pre-reaction) to − 12.2 mV (unwashed) and − 8.43 mV (washed) after reaction (Table 2), confirming adsorption of tetramethoxyborate ($[B(OCH_3)_4]^-$) anions onto quaternized nitrogen sites of P(Q-DMA). This dynamic surface modification supports the view that synergistic ion–ion, ion–dipole, and hydrogen bonding interactions collectively lower the activation barrier. This observation is in line with previous reports on protonated chitosan–zeolite hybrids, where positively charged $–NH_3^+$ groups and acidic zeolite sites promoted BH_4^- adsorption and proton transfer, thereby enhancing hydrogen generation efficiency [18]. Furthermore, the zwitterionic structure of P(Q-DMA) provides a synergistic framework where quaternized ammonium cations and sulfonate anions function cooperatively. This dual-site configuration enables simultaneous stabilization of $NaBH_4$ and MeOH, ensuring efficient adsorption and charge transfer. The concurrent presence of hydrogen-bonding ester and sulfonate groups

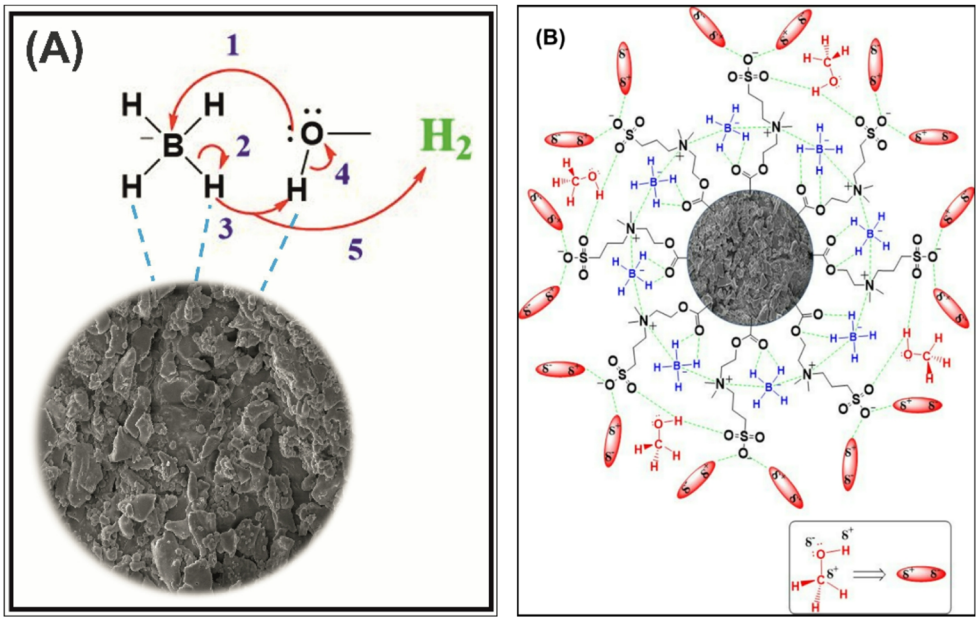

Fig. 11 Proposed catalytic mechanism of P(Q-DMA) (A) and adsorption mechanism of MeOH and $NaBH_4$ on P(Q-DMA) (B), based on experimental observations (zeta potential, FTIR) and supported by DFT calculations

amplifies this effect by stabilizing reactive intermediates. As a result, the catalyst benefits from a collective reduction in activation energy and a marked enhancement in hydrogen generation rates. The proposed catalytic mechanism was further validated through DFT calculations, confirming the above interactions and processes. These results highlight the combined effects of electrostatic interactions, hydrogen bonding, and ion–dipole interactions in driving the superior catalytic performance of P(Q-DMA) in $NaBH_4$ methanolysis. In addition, the structural modifications introduced by the zwitterionic architecture of P(Q-DMA) directly correlate with its catalytic performance. The presence of both quaternized ammonium cations and sulfonate anions creates multiple active interaction sites, enhancing adsorption and charge transfer between $NaBH_4$ and MeOH. The ester and sulfonate groups further contribute through strong hydrogen bonding, which stabilizes intermediates and lowers the activation barrier. SEM analysis confirmed irregular nanoscale morphologies that increase surface accessibility, while zeta potential measurements demonstrated the adsorption of borohydride-derived species, validating dynamic charge modulation during the reaction. Collectively, these structural features explain the observed low activation energy (19.91 kJ mol^{-1}), high hydrogen generation rate (8868.4 mL H_2 min^{-1} $g_{cat}{}^{-1}$), and operational stability, thereby establishing a clear structure–performance relationship unique to P(Q-DMA). Such effects are consistent with previous findings that nitrogen and oxygen functionalities in carbon frameworks facilitate adsorption and charge transfer during $NaBH_4$ methanolysis [19].

To provide a more detailed mechanistic insight, the catalytic pathway of P(Q-DMA) in $NaBH_4$ methanolysis can be described in four sequential stages (Fig. 11):

(i) Adsorption – $NaBH_4$ is electrostatically attracted to quaternized ammonium sites, while MeOH interacts with sulfonate groups via ion–dipole interactions.
(ii) Activation of reactants – Quaternized ammonium groups polarize the B–H bonds of $NaBH_4$, whereas sulfonate and ester groups form hydrogen bonds with MeOH, lowering the activation barrier.
(iii) Intermediate formation and H_2 release – MeOH molecules attack the boron atom, leading to B–H bond cleavage; simultaneously, hydrides from $NaBH_4$ react with protons of MeOH to generate H_2.
(iv) Product desorption and regeneration –$[B(OCH_3)_4]^-$ intermediates remain weakly adsorbed on ammonium sites, while H_2 molecules are freely released due to weak van der Waals interactions, as supported by DFT calculations.

This stepwise mechanism demonstrates how the synergistic interactions within P(Q-DMA) facilitate efficient hydrogen evolution while maintaining catalyst stability.

3.2.6 Computational Results

Many different initial structures were created manually to determine lowest energy positions of methanol, BH_4^- and H_2 solvent on the model structure that represents functional groups on the polymer. The four lowest energy structures for model polymer-methanol and their counterpoise corrected interaction energies are given in Fig. 12. These results presented that MeOH is mainly coordinated with the sulfonate anion head group followed the coordination around the ester group.

This calculation is repeated for all groups on the same polymer model structure and lowest energy structures with highest interaction energies were determined (Fig. 13). We determined that while the MeOH coordinated with the sulfonate group, the strongest interaction energy is determined for BH_4^- with the tertiary ammonium cation with −43.82 kcal mol^{-1} interaction energy. The weakest interaction energy is determined for the H_2 interaction with the model structure at less than 2 kcal/mol that indicates the relatively free movement of the H_2 molecules in the system.

In addition to the pairwise interactions; model unit, methanol, BH_4^- and H_2 were optimized all together in the same system starting from different initial structures. We determined that the molecules conserved their positions and interaction energies in the lowest energy structure (Fig. 14) with a slight decrease compared to the energies and position calculated in the pairwise interactions given in Fig. 13.

It should be noted that our calculations showed that the BH_4^- interaction with the quarternary ammonium groups have the strongest interaction energy and the second lowest energy for the same system have very significant difference with this lowest energy polymer-BH_4^- interaction. The position of BH_4^- is decisive around ammonium cation. Oppositely, H_2 have very low interaction energy with close values between 1–2 kcal mol^{-1} freely moving in the system. For methanol solvent, we concluded that while they were mainly concentrated around the sulfonate group with the interaction energy over 20 kcal mol^{-1}, it is also possible to interact partly with ester group of the polymer with interaction energy around 10 kcal mol^{-1}. The lowest energy structure for five methanol groups around the model polymer unit confirm this result given in Fig. 15 which show four of the methanol is in interaction with the sulfonate group and one of the is in interaction with ester group. We demonstrated that the polymer unit can coordinate one BH_4^- strongly and many MeOH solvents with significant hydrogen bond interactions. H_2 molecules are freely moving in the polymer network with weak vdW interaction.

3.2.7 Comparison with Literature

In order to better evaluate this study, the results obtained were compared with other studies in the literature (Table 1). The results were compared in terms of HGR. However, two HGR values were compared, one with the catalyst amount (mL H_2 min^{-1}) and one without it (mL H_2 min^{-1} g^{-1}). When the catalyst amount is included in the HGR calculation, the HGR value decreases with the increase in the catalyst amount. The lower the catalyst amount used, the higher the HGR values are achieved. This does not provide sufficient precision in terms of comparing the results with the literature. For example, in this study, while the maximum HGR

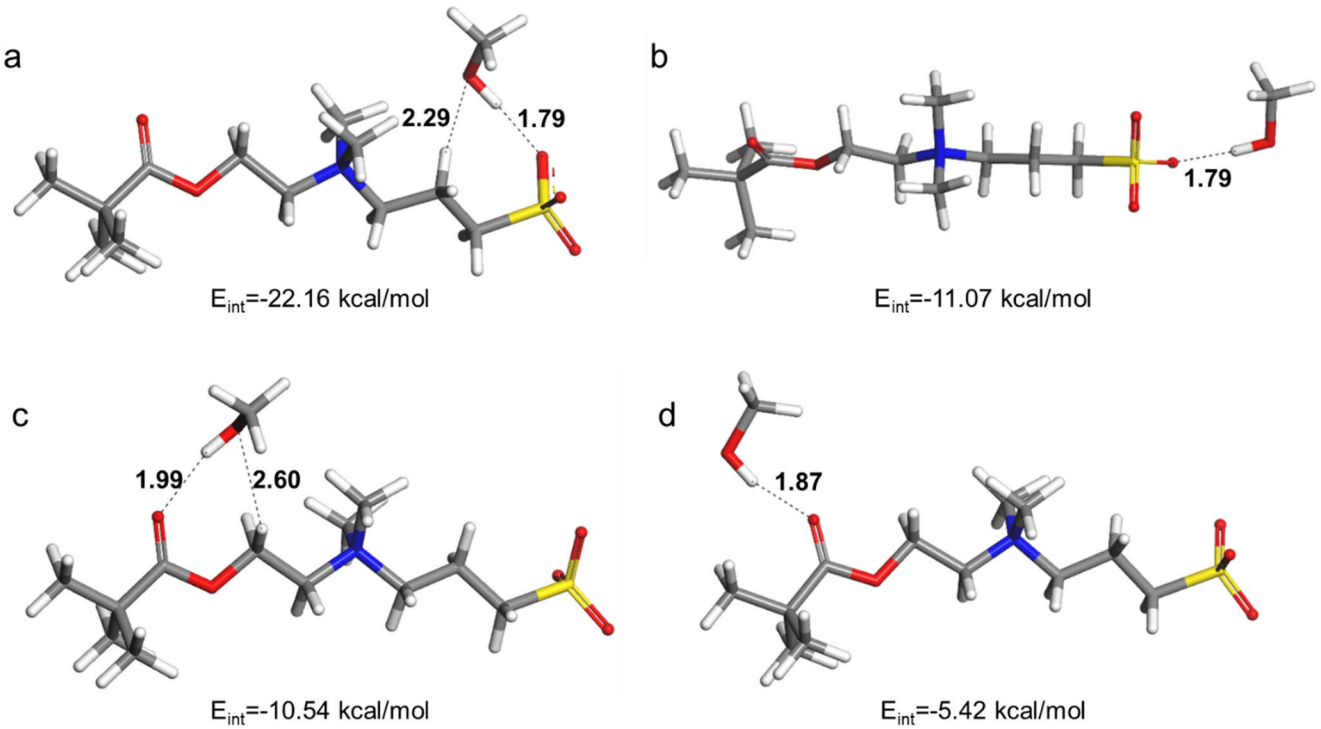

Fig. 12 Optimized structures and corresponding interaction energies for the four lowest-energy configurations illustrating the adsorption of methanol on the model repeating unit of the P(Q-DMA). (a) methanol forming hydrogen bonds with the sulfonate oxygen and a backbone C–H hydrogen atom, (b) methanol coordinated mainly with the sulfonate group, (c) methanol interacting simultaneously with a carbonyl oxygen and a backbone C–H hydrogen atom, and (d) methanol forming a single hydrogen bond with a carbonyl oxygen.

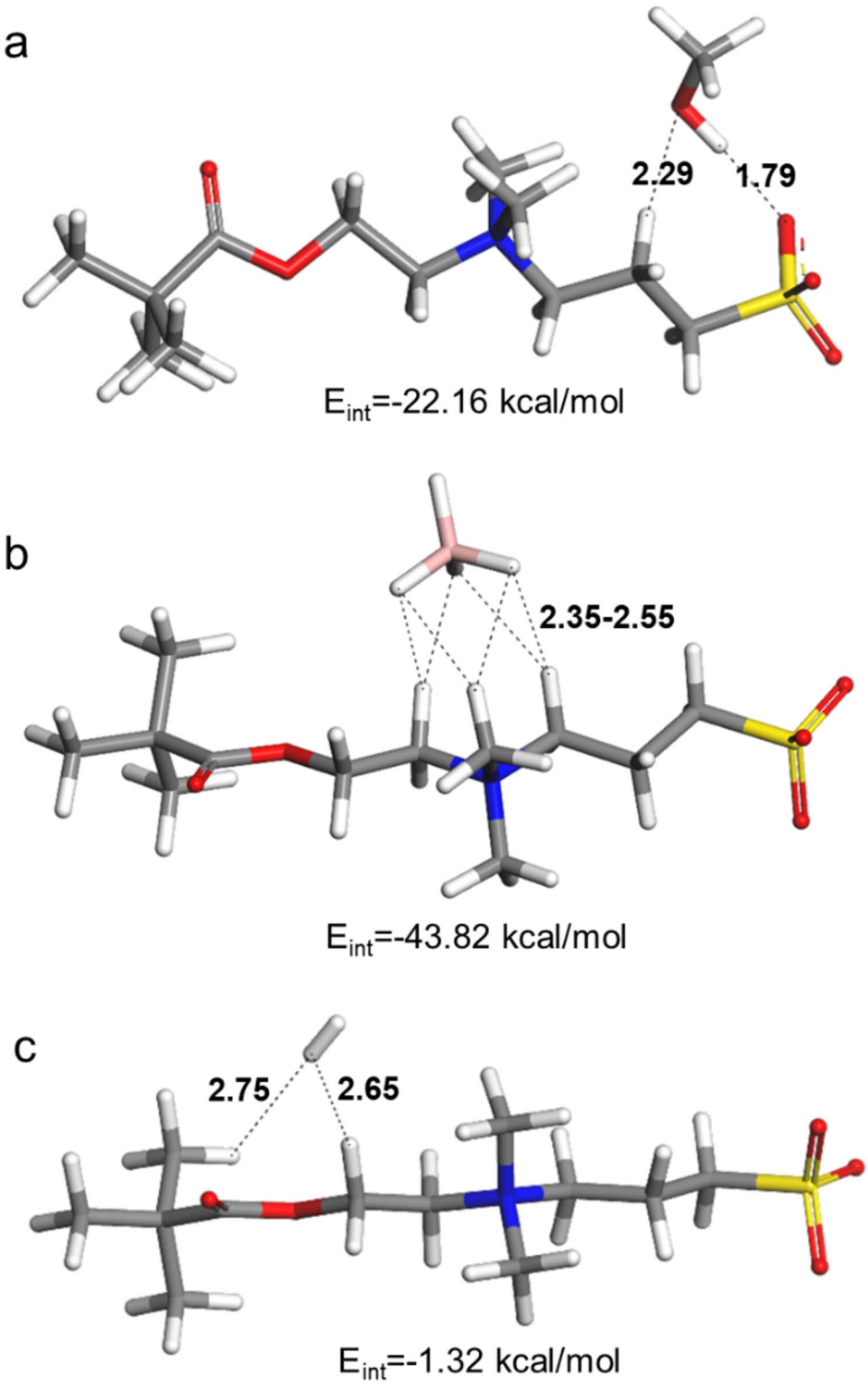

Fig. 13 Lowest energy structures and their interaction energies for these structures for **a)** methanol, **b)**BH_4^- and **c)** H_2

value of 8868.4 mL H_2 min^{-1} g^{-1} was achieved with P(Q-DMA), Gokkus et al. [43] obtained a maximum HGR value of 39,459.6 mL H_2 min^{-1} g^{-1} with GD particles. In other words, while GD particles had 4.45 times better catalytic performance than P(Q-DMA), when the amount of catalyst was removed from these calculations, the hydrogen production rate of P(Q-DMA) was 443.4 mL H_2 min^{-1} and that of GD particles was 394.6 mL H_2 min^{-1}. Accordingly, it was understood that P(Q-DMA) actually had better catalytic performance than GD particles. For this reason, HGR values

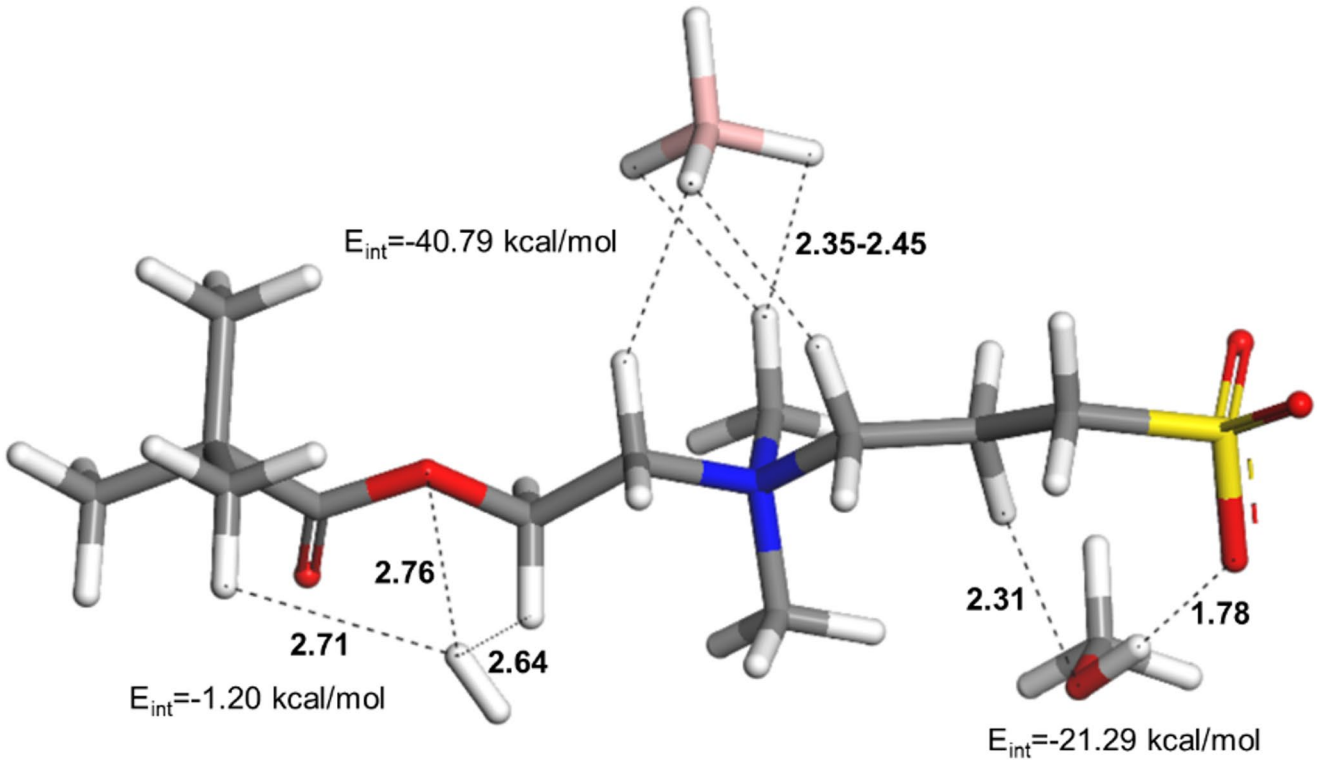

Fig. 14 Lowest energy structure and interaction energy for the system containing model unit, methanol, BH_4^- and H_2 together

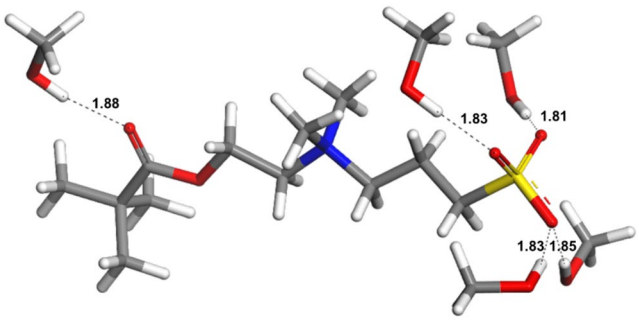

Fig. 15 Lowest energy structure and interaction energy for the system containing model unit, and five methanol

obtained without including the amount of catalyst were also included in the comparisons.

In terms of HGR values (mL H_2 min^{-1} g^{-1}), the HGR achieved with P(Q-DMA) (8868.36 mL H_2.$min^{-1}g_{cat}^{-1}$) was found to be significantly higher than many studies in the literature (Table 1). When Table 1 was examined, it was seen that the HGR values (21,960.2, 39,459.6, 20,425, 10,027, and 9716.3 mL H_2 $min^{-1}g_{cat}^{-1}$) obtained with TD and GD particles [43], natural lignin [12], F1 [44] and Carbon nanotube (CNT) supported bimetallic CuBi [45] catalysts, respectively, were higher than P(Q-DMA. The activation energies of these catalysts were found to be 16.86, 18.14, 19.5, 18.21 and 34.72 kJ mol^{-1}, respectively. TD and GD particles contain amine groups and hydroxyl groups that have the ability to make strong hydrogen bonds in their structures. It was demonstrated by Sahiner and his group that the catalytic effects of amine groups in hydrogen production were quite high [3, 4, 7, 8, 46]. Natural lignin contains hydroxyl, carbonyl, ether and phenyl groups that have the capacity to make abundant hydrogen bonds. It was thought that the high effect of these groups led to both a significant increase in the HGR values of the catalysts and a decrease in their Ea values. This provided higher results than P(Q-DMA).

In terms of HGR (mL H_2 min^{-1}), it was understood that the HGR values calculated with natural lignin (1021.2 mL H_2 min^{-1}) [12], TD particles (549 mL H_2 min^{-1}) [43], F1 (501.35 mL H_2 min^{-1}) [44] and carbon nanotube (CNT) supported bimetallic CuBi (485.6 mL H_2 min^{-1}) [45] were higher than 443.4 mL H_2 min^{-1} obtained for P(Q-DMA). As stated above, natural lignin and TD particles are quite

Table 2 Zeta potential values of P(Q-DMA) before and after $NaBH_4$ methanolysis

Zeta potentials (mV)			
	Before H_2 production	After H_2 production (unwashed)	After H_2 production (washed)
P(Q-DMA)	13.1	−12.2	−8.43

Conditions: T = 25 °C, Solvent; Methanol

rich in hydroxyl and amine groups that will make strong hydrogen bonds. It is thought that these catalysts may have shown better catalytic performance due to this effect. On the other hand, it was seen that F2 had the same catalytic effect as P(Q-DMA) in terms of both HGR values (441.9, and 8839 mL H_2 min^{-1}) [44]. Moreover, the HGR values obtained with AAPC-WBTL and AAPC-WGTL (7676, and 9084.75 mL H_2 min^{-1}, respectively) [47] were quite close to P(Q-DMA) and therefore their catalytic effects seemed to be close to each other. However, when in terms of HGR, the rates of AAPC-WBTL and AAPC-WGTL being 76.76, and 90.85 mL H_2 min^{-1}, respectively, revealed that these two catalysts had considerably lower performance in hydrogen production compared to P(Q-DMA). In fact, when in terms of HGR values, it was clearly seen that P(Q-DMA) had considerably higher catalytic performance as a catalyst in hydrogen production compared to the literature.

On the other hand, when Table 1 is examined in terms of E_a values, it was found that three catalysts [9, 25, 39] had lower E_a values than P(Q-DMA). However, their HGR values were lower than those obtained with P(Q-DMA). Based on these comparisons, it is concluded that P(Q-DMA) was a better catalyst. Furthermore, incorporating different groups capable of forming hydrogen bonds into the structure of P(Q-DMA) could lead to much higher catalytic performance. In light of these comparisons and evaluations, it was seen that P(Q-DMA) offers significant insights into hydrogen production via methanolysis of $NaBH_4$.

3.2.8 Correlation of Zeta Potential with Morphology and Textural Properties

To better understand the effect of surface charge on catalytic performance, zeta potential measurements were carried out before and after $NaBH_4$ methanolysis (Table 2). These measurements not only reveal the dynamic surface modifications of the catalyst but also provide a link between its structural properties and catalytic efficiency. Before the reaction, the catalyst exhibited a positive zeta potential of + 13.1 mV, attributed to the presence of quaternary ammonium groups. After the reaction, a pronounced decrease was observed, with values of − 12.2 mV for unwashed samples and − 8.43 mV for washed samples. This shift indicates the adsorption of borate species such as tetramethoxyborate ($[B(OCH_3)_4]^-$) onto the polymer surface, leading to a reversal of surface charge and confirming dynamic surface modification during catalysis.

The correlation between morphology, textural properties, and zeta potential further supports this observation. SEM images revealed irregular nano- to microscale particle morphologies, enhancing surface accessibility. BET analysis showed that the catalyst possessed a relatively high surface area and pore volume, which facilitated the exposure of active sites and promoted ion–dipole and hydrogen-bonding interactions with $NaBH_4$ and methanol. These structural features, together with the observed zeta potential changes, demonstrate that the functional groups (quaternary ammonium, sulfonate, and ester) operate synergistically to stabilize intermediates and enhance catalytic activity. Overall, the catalytic performance of P(Q-DMA) can be attributed not only to its chemical functionality but also to the interplay of surface charge distribution, porosity, and morphology. The positive-to-negative shift in zeta potential is consistent with other reports on biopolymeric and heteroatom-doped carbon systems, further confirming strong borate adsorption. These correlations explain the experimentally observed low activation energy (19.91 kJ mol^{-1}) and high hydrogen generation rate (8868.4 mL H_2 min^{-1} g_{cat}^{-1}), providing a clear structure–property relationship that underpins the superior efficiency of P(Q-DMA). These findings suggest that tuning surface charge alongside morphological design could be a promising strategy for the development of next-generation, metal-free polymeric catalysts for H_2 production.

3.2.9 Electrochemical Results

The electrocatalytic activity of P(Q-DMA) for $NaBH_4$ electrooxidation was determined by CV measurements taken at 50 mV/s scan rate in the range of − 0.8–0.8 V. The CV curves of the measurements carried out in two different solutions, 1 M NaOH and 1 M NaOH + 0.1 M NaBH4, are compared in Fig. 16a. When the CV curves were examined, it was seen that no distinct peak belonging to sodium borohydride oxidation was obtained in the forward scan region. Therefore, the electrocatalytic activity of the polymer was evaluated over the total current and the specific activity was obtained as 0.72 mA cm^{-2}.

CA electrochemical measurements for the stability of the polymer in sodium borohydride electrooxidation were applied at different voltage values such as 0.0; 0.2; 0.4; 0.6; 0.8 V for 1000 s. According to the CA curves given in Fig. 16b, initially a rapid decrease occurred due to the poisoning of the electrode surface, then the current value remained constant. The longest period of stability was achieved at 0.8 V. EIS measurements, which determined the resistance of the polymer to sodium borohydride electrooxidation, were evaluated with Nyquist curves in Fig. 16c. Nyquist curves give information about the charge transfer resistance and have a semicircular shape. Since the charge transfer resistance decreases as the diameter of the semicircle decreases, the lowest charge transfer resistance was achieved for the polymer at 0.8 V.

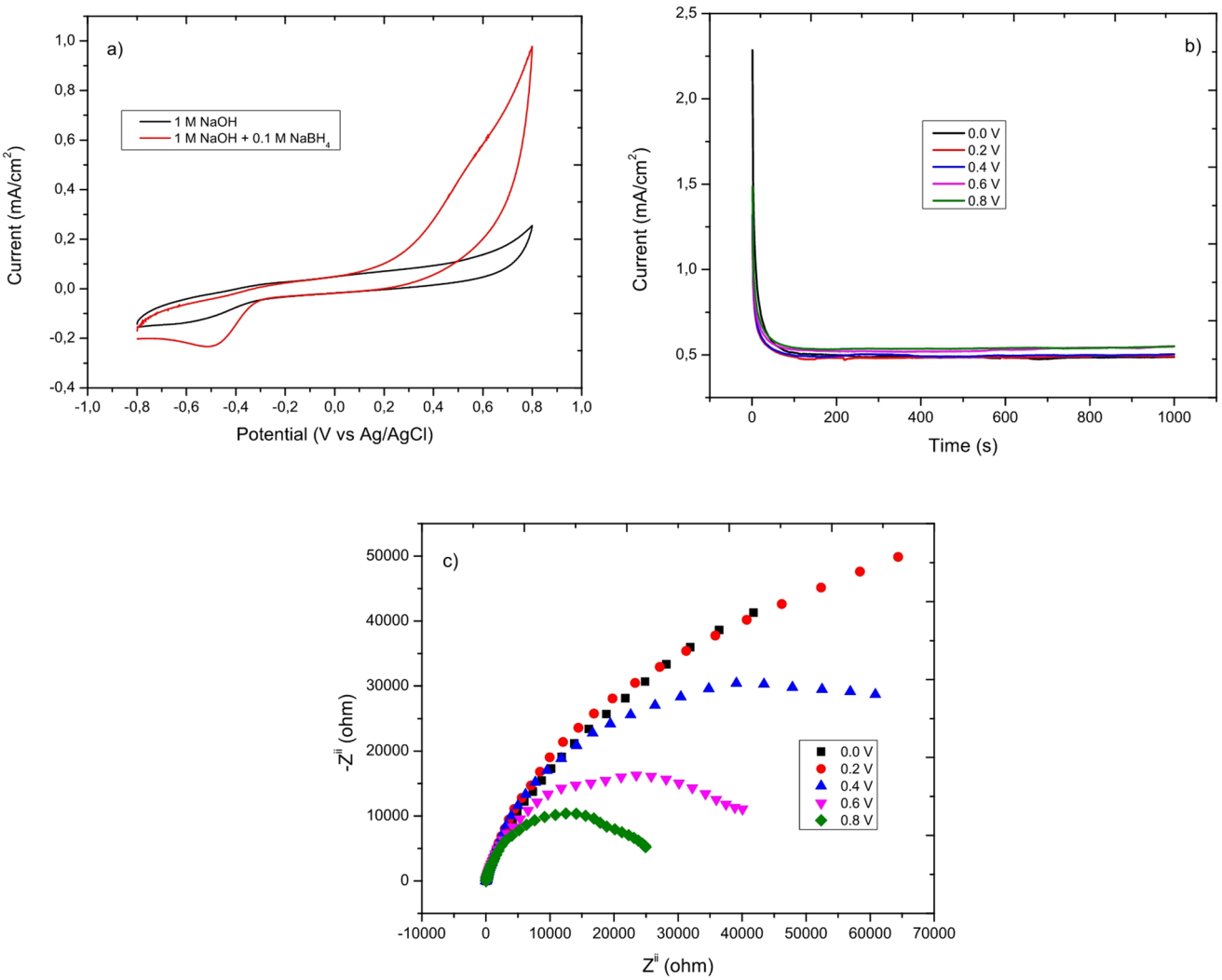

Fig. 16 Electrochemical results of P(Q-DMA) polymer **(a)** CV results at 50 mV s^{-1} scan rate, **(b)** CA results of the polymer at different voltages and **(c)** Nyquist plots at different voltages. (Experimental conditions: 0.1 M $NaBH_4$ in 0.5 M NaOH, scan rate 50 mV s^{-1}, potential range 0–1.0 V)

4 Conclusion

The experimental results confirmed that the synthesized zwitterionic polymer, P(Q-DMA), exhibits superior catalytic performance in $NaBH_4$ methanolysis compared to conventional catalysts. It achieved a high hydrogen generation rate (443.4 mL H_2 min^{-1} and 8868.4 mL H_2 min^{-1} $g_{cat}{}^{-1}$) under mild conditions, along with a low activation energy (19.91 kJ mol^{-1}). These findings demonstrate the catalyst's ability to facilitate hydrogen release efficiently while reducing energy demand, in line with green chemistry principles. This work represents the first demonstration of P(Q-DMA) as a metal-free catalyst, enabled by its unique zwitterionic architecture that promotes synergistic ion–ion, ion–dipole, and hydrogen-bonding interactions. These interactions were validated by both DFT calculations and experimental observations, including zeta potential measurements. Notably, the surface charge shifted from + 13.1 mV before reaction to − 12.2 mV (unwashed) and − 8.43 mV (washed) after reaction, confirming borate adsorption and dynamic surface modification. Compared to previously reported systems such as TD/GD particles and lignin-based catalysts, P(Q-DMA) provides an environmentally safer alternative, balancing catalytic efficiency with structural simplicity. Although some metal-containing catalysts exhibit slightly lower activation energies, the biodegradable and metal-free nature of P(Q-DMA) directly addresses concerns related to toxicity, resource scarcity, and environmental impact. Looking ahead, future studies should focus on tailoring the polymer structure to further enhance catalytic efficiency, scaling up synthesis for industrial hydrogen production, and integrating waste-heat recovery with life-cycle assessments to maximize sustainability. Coupling P(Q-DMA)-based systems with renewable energy sources such as photovoltaics

and wind power could accelerate progress toward circular economy and net-zero-emission goals. By bridging experimental validation with theoretical modeling, this work establishes a solid foundation for the development of robust, eco-friendly, and scalable polymer-based catalysts to meet the growing demand for clean hydrogen energy.

Acknowledgements We would like to thank the Scientific and Technological Research Council of Türkiye (TUBITAK) for supporting this study with research project number 118C466. The numerical calculations reported in this paper were partially performed at TUBITAK ULAKBIM, High Performance and Grid Computing Center (TRUBA resources).

Author Contributions K.G. and V.B. contributed to the conceptualization and experimental design of the study. K.G. also performed the synthesis and hydrogen generation experiments. S.K. conducted supporting experimental work. M.G. was involved in experimental procedures and material characterization. D.Y. and H.K. carried out electrochemical measurements. E.Y. performed the DFT calculations and contributed to theoretical interpretation. All authors contributed to the writing of the manuscript and approved the final version.

Funding The authors did not receive support from any organization for the submitted work.

Data Availability The data that support the findings of this study are available from the corresponding author upon reasonable request.

Declarations

Competing Interests The authors declare that they have no known competing financial interests or personal relationships that could have appeared to influence the work reported in this paper.

Ethical Approval Not applicable.

Consent to Participate Not applicable.

Consent for Publication Not applicable.

References

1. Monteverde M, Magistri L (2012) Hydrogen from sodium borohydride and fossil source: an energetic and economical comparison. Int J Hydrogen Energy 37:5452–5460. https://doi.org/10.1016/J.IJHYDENE.2011.09.047
2. Kumar R, Singh R, Dutta S (2024) Review and outlook of hydrogen production through catalytic processes. Energy Fuels 38:2601–2629. https://doi.org/10.1021/ACS.ENERGYFUELS.3C04026/ASSET/IMAGES/MEDIUM/EF3C04026_0010.GIF
3. Sahiner N, Yasar AO, Aktas N (2017) Metal-free pyridinium-based polymeric ionic liquids as catalyst for H_2 generation from $NaBH_4$. Renew Energy 101:1005–1012. https://doi.org/10.1016/j.renene.2016.09.066
4. Sahiner N (2018) Carbon spheres from lactose as green catalyst for fast hydrogen production via methanolysis. Int J Hydrogen Energy 43:9687–9695. https://doi.org/10.1016/j.ijhydene.2018.04.050
5. Sahiner N, Yasar AO (2016) Imidazolium based polymeric ionic liquid microgels as an alternative catalyst to metal catalysts for H_2 generation from methanolysis of $NaBH_4$. Fuel Process Technol 152:316–324. https://doi.org/10.1016/J.FUPROC.2016.06.023
6. Sahiner N, Sengel SB (2017) Environmentally benign halloysite clay nanotubes as alternative catalyst to metal nanoparticles in H_2 production from methanolysis of sodium borohydride. Fuel Process Technol 158:1–8. https://doi.org/10.1016/J.FUPROC.2016.12.009
7. Sahiner N, Sengel SB (2017) Various amine functionalized halloysite nanotube as efficient metal free catalysts for H_2 generation from sodium borohydride methanolysis. Appl Clay Sci 146:517–525. https://doi.org/10.1016/j.clay.2017.07.008
8. Sahiner N, Sengel SB (2016) Quaternized polymeric microgels as metal free catalyst for H_2 production from the methanolysis of sodium borohydride. J Power Sources 336:27–34. https://doi.org/10.1016/j.jpowsour.2016.10.054
9. Demirci S, Sutekin SD, Guven O, Sahiner N (2023) Poly(2-aminoethyl methacrylate) based microgels catalyst system to be used in hydrolysis and methanolysis of $NaBH_4$ for H_2 generation. Int J Hydrogen Energy 48:23002–23012. https://doi.org/10.1016/J.IJHYDENE.2023.02.091
10. Abebe MW, Baye AF, Kim H (2022) Poly(acrylic acid)/polysaccharides IPN derived metal free catalyst for rapid hydrogen generation via $NaBH_4$ methanolysis. Int J Hydrogen Energy 47:32060–32070. https://doi.org/10.1016/j.ijhydene.2022.07.106
11. Baytar O, Şahin Ö, Ekinci A (2023) Effect of environmentally friendly and efficient metal-free hydrochars as catalysts on sodium borohydride hydrolysis. Fuel. https://doi.org/10.1016/j.fuel.2023.128308
12. Ma M, Zhou W, Zhang Y, Huang Q, Hu Z, Ouyang L (2024) Natural lignin as efficient catalyst for H_2 production from $NaBH_4$ methanolysis at low temperature. J Environ Chem Eng. https://doi.org/10.1016/j.jece.2023.111615
13. Onat E, Ahmet Celik F, Şahin Ö, Karabulut E, Izgi MS (2024) H_2 production from ammonia borane hydrolysis with catalyst effect of Titriplex® III carbon quantum dots supported by ruthenium under different reactant conditions: experimental study and predictions with molecular modelling. Chem Eng J 497:154593. https://doi.org/10.1016/J.CEJ.2024.154593
14. Onat E, İzgi MS, Şahin Ö, Ekinci S (2025) Enhanced hydrogen production from sucrose-derived carbon quantum dots-supported Ru catalysts: a comparative study of KBH_4 and $NaBH_4$ hydrolysis. Renew Energy 254:123692. https://doi.org/10.1016/J.RENENE.2025.123692
15. Saka C (2023) Nitrogen and oxygen heteroatom doping with hydrothermal nitric acid treatment on the catalytic performance of metal-free carbon particles: hydrogen release from sodium borohydride in methanol. Catal Lett 153:3734–3749. https://doi.org/10.1007/S10562-023-04277-3/METRICS
16. Saka C (2022) Facile fabrication of P-doped g-C_3N_4 particles with nitrogen vacancies for efficient dehydrogenation of sodium borohydride methanolysis. Fuel 313:122688. https://doi.org/10.1016/J.FUEL.2021.122688
17. Onat E, Ekinci S, Şahin Ö, İzgi MS (2025) Effective and environmentally friendly Co nanocatalyst on sodium borohydride hydrolysis in different solvents. Int J Hydrogen Energy 142:864–874. https://doi.org/10.1016/J.IJHYDENE.2025.01.073
18. Saka C (2023) Highly active hydrogen generation from sodium borohydride methanolysis and ethylene glycolysis reactions using protonated chitosan-zeolite hybrid metal-free particles. Appl Catal B 325:122335. https://doi.org/10.1016/J.APCATB.2022.122335
19. Saka C, Balbay A (2021) Oxygen and nitrogen-functionalized porous carbon particles derived from hazelnut shells for the

efficient catalytic hydrogen production reaction. Biomass Bioenergy 149:106072. https://doi.org/10.1016/J.BIOMBIOE.2021.106072
20. Saka C (2021) Metal-free catalysts with phosphorus and oxygen doped on carbon-based on *Chlorella vulgaris* microalgae for hydrogen generation via sodium borohydride methanolysis reaction. Int J Hydrogen Energy 46:5150–5157. https://doi.org/10.1016/j.ijhydene.2020.09.220
21. Alpaslan D, Ersen Dudu T, Aktas N (2023) Synthesis of poly(ginger oil) organo particles as a metal free catalysis and their use in hydrogen production from sodium borohydride methanolysis. J Polym Environ 31:1191–1201. https://doi.org/10.1007/s10924-022-02636-6
22. Gokkus K, Gür M, Bütün V (2024) Synthesis and characterization of azo cross-linked polymer as a new catalyst for the production of hydrogen gas by methanolysis of $NaBH_4$. J Appl Polym Sci 141:e56051. https://doi.org/10.1002/APP.56051
23. Pérez JPH, López-Cabarcos E, López-Ruiz B (2010) Amperometric glucose biosensor based on biocompatible poly(dimethylaminoethyl) methacrylate microparticles. Talanta 81:1197–1202. https://doi.org/10.1016/j.talanta.2010.02.010
24. Ajkidkarn P, Ritprajak P, Injumpa W, Porntaveetus T, Insin N (2017) Synthesis, characterization, drug release and transdentinal delivery studies of magnetic nanocubes coated with biodegradable poly(2-(dimethyl amino)ethyl methacrylate). J Magn Magn Mater 427:235–240. https://doi.org/10.1016/j.jmmm.2016.11.020
25. Bütün V, Armes SP, Billingham NC (2001) Selective quaternization of 2-(dimethylamino)ethyl methacrylate residues in tertiary amine methacrylate diblock copolymers. Macromolecules 34:1148–1159. https://doi.org/10.1021/ma001550k
26. Bütün V (2003) Selective betainization of 2-(dimethylamino) ethyl methacrylate residues in tertiary amine methacrylate diblock copolymers and their aqueous solution properties. Polymer (Guildford) 44:7321–7334. https://doi.org/10.1016/J.POLYMER.2003.09.027
27. Stephens PJ, Devlin FJ, Chabalowski CF, Frisch MJ (1994) Ab initio calculation of vibrational absorption and circular dichroism spectra using density functional force fields. J Phys Chem® 98:11623–11627. https://doi.org/10.1021/J100096A001/ASSET/J100096A001.FP.PNG_V03
28. Frisch MJ ea, Trucks GW, Schlegel HB, Scuseria GE, Robb Ma, Cheeseman JR et al (2016) Gaussian 16
29. Grimme S, Antony J, Ehrlich S, Krieg H (2010). A consistent and accurate ab initio parametrization of density functional dispersion correction (DFT-D) for the 94 elements H-Pu. J Chem Phys. https://doi.org/10.1063/1.3382344/926936
30. Tomasi J, Mennucci B, Cammi R (2005) Quantum mechanical continuum solvation models. Chem Rev 105:2999–3093. https://doi.org/10.1021/CR9904009/ASSET/CR9904009.FP.PNG_V03
31. van Duijneveldt FB, van Duijneveldt-van de Rijdt JGCM, van Lenthe JH (1994) State of the art in counterpoise theory. Chem Rev 94:1873–1885. https://doi.org/10.1021/CR00031A007/ASSET/CR00031A007.FP.PNG_V03
32. Caglar A, Kaya S, Saka C, Yildiz D, Kivrak H (2024) Investigation of electrooxidation and methanolysis of sodium borohydride on activated carbon supported Co catalysts from poplar sawdust. Int J Hydrogen Energy 75:171–178. https://doi.org/10.1016/J.IJHYDENE.2024.01.083
33. Xu C, Hu M, Wang Q, Fan G, Wang Y, Zhang Y et al (2018) Hyper-cross-linked polymer supported rhodium: an effective catalyst for hydrogen evolution from ammonia borane. Dalton Trans 47:2561–2567. https://doi.org/10.1039/C7DT04549B
34. Dudu TE, Alpaslan D, Aktas N (2022) Hydrogen production from methanolysis of sodium borohydride by non-metal p(CO) organo-particles synthesized from castor oil. J Polym Environ 30:4562–4570. https://doi.org/10.1007/s10924-022-02521-2
35. Tercan M, Karacan Yeldir E, Dayan O, Oral A (2020) P(2-VP) supported Ru(II) material as catalyst for H_2 production from the methanolysis of $NaBH_4$. Inorg Nano-Met Chem 50:1343–1352. https://doi.org/10.1080/24701556.2020.1749077
36. Inger E, Sunol AK, Sahiner N (2020) Catalytic activity of metal-free amine-modified dextran microgels in hydrogen release through methanolysis of $NaBH_4$. Int J Energy Res 44:5990–6001. https://doi.org/10.1002/er.5395
37. Liao J, Shao Y, Feng Y, Zhang J, Song C, Zeng W et al (2023) Interfacial charge transfer induced dual-active-sites of hetero-structured $Cu_{0.8}Ni_{0.2}WO_4$ nanoparticles in ammonia borane methanolysis for fast hydrogen production. Appl Catal B 320:121973. https://doi.org/10.1016/J.APCATB.2022.121973
38. Su CC, Lu MC, Wang SL, Huang YH (2012) Ruthenium immobilized on Al_2O_3 pellets as a catalyst for hydrogen generation from hydrolysis and methanolysis of sodium borohydride. RSC Adv 2:2073–2079. https://doi.org/10.1039/C2RA01233B
39. Shiferraw BT, Baye AF, Kim H (2024) Mechanistic insights into the deprotonation of methanol by facile synthesized 3D flower-like BiO_X (X= Cl, Br, I) catalysts for rapid hydrogen generation from $NaBH_4$ methanolysis: the 'X' factor. Int J Hydrogen Energy 51:435–450. https://doi.org/10.1016/J.IJHYDENE.2023.08.212
40. Santra S, Das D, Das NS, Nanda KK (2017) An efficient on-board metal-free nanocatalyst for controlled room temperature hydrogen production. Chem Sci 8:2994–3001. https://doi.org/10.1039/C7SC00162B
41. Sahiner N, Demirci S (2017) Natural microgranular cellulose as alternative catalyst to metal nanoparticles for H_2 production from $NaBH_4$ methanolysis. Appl Catal B 202:199–206. https://doi.org/10.1016/j.apcatb.2016.09.028
42. Saka C (2021) Phosphorus and oxygen doped carbon-based on *Spirulina* microalgae as efficient metal-free catalysts to obtain H_2 from methanolysis of $NaBH_4$. Int J Hydrogen Energy 46:3753–3762. https://doi.org/10.1016/j.ijhydene.2020.08.222
43. Gokkus K, Kaya S, Yildiz D, Saka C, Gür M, Bütün V et al (2024) Synthesis and characterization of polymer particles as metal-free catalysts for electrooxidation and methanolysis of sodium borohydride. ChemistrySelect. https://doi.org/10.1002/slct.202304975
44. Rüzgar D, Yıldız D, Kaya Ş, verdu Martinez J, Yeşilbursa G, Demir Kıvrak H (2024) Waste ceramic frit as novel catalyst triggering sodium borohydride methanolysis reaction. Int J Hydrogen Energy 56:1038–1048. https://doi.org/10.1016/j.ijhydene.2023.12.213
45. Abbas MJA, Caglar A, Kivrak H (2024) The synthesis and characterization of carbon nanotube-supported CuBi catalyst for H_2 production from $NaBH_4$ methanolysis. Process Saf Environ Prot 185:96–104. https://doi.org/10.1016/j.psep.2024.03.020
46. Demirci S, Zekoski T, Sahiner N (2019) The preparation and use of p(2-acrylamido-2-methyl-1-propanesulfonic acid)-tris(dioxa-3,6-heptyl)amine (p(AMPS)-TDA-1) ionic liquid microgel in hydrogen production. Polym Bull 76:1717–1735. https://doi.org/10.1007/S00289-018-2465-0/FIGURES/7
47. Srivastava N, Pal N, Agarwal M, Dohare RK (2023) Investigation of the performance of metal-free catalyst prepared from black tea and green tea waste for hydrogen production via methanolysis of sodium borohydride and optimization using response surface methodology. Int J Hydrogen Energy 48:35919–35937. https://doi.org/10.1016/J.IJHYDENE.2023.05.356

Authors and Affiliations

Kutalmis Gokkus[1] · Sefika Kaya[2] · Mahmut Gür[3] · Derya Yildiz[2] · Erol Yıldırım[4] · Hilal Kivrak[2] · Vural Bütün[5]

✉ Mahmut Gür
mahmutgur@kastamonu.edu.tr

[1] Department of Environmental Engineering, Faculty of Engineering and Architecture, Kastamonu University, Kuzeykent, 37500 Kastamonu, Turkey

[2] Department of Chemical Engineering, Faculty of Engineering and Architectural Sciences, Eskisehir Osmangazi University, Meselik Campus, 26040 Eskisehir, Turkey

[3] Department of Forest Industrial Engineering, Faculty of Forest, Kastamonu University, Kuzeykent, 37500 Kastamonu, Turkey

[4] Department of Chemistry, Middle East Technical University, 06800 Ankara, Turkey

[5] Department of Chemistry, Faculty of Science, Eskisehir Osmangazi University, Meselik Campus, 26480 Eskisehir, Turkey